

Reconciling PTA and JWST and preparing for LISA with POMPOCO: a Parametrisation Of the Massive black hole POpulation for Comparison to Observations

A. Toubiana^{1,2,3}, L. Sberna⁴, M. Volonteri⁵, E. Barausse^{6,7}, S. Babak⁸, R. Enficiaud¹, D. Izquierdo-Villalba^{2,3}, J. R. Gair¹, J. E. Greene⁹, and H. Quelquejey Leclere⁸

¹ Max Planck Institute for Gravitationsphysik (Albert Einstein Institute), Am Mühlenberg 1, 14476 Potsdam, Germany

² Dipartimento di Fisica “G. Occhialini”, Università degli Studi di Milano-Bicocca, Piazza della Scienza 3, 20126 Milano, Italy

³ INFN, Sezione di Milano-Bicocca, Piazza della Scienza 3, 20126 Milano, Italy

⁴ School of Mathematical Sciences, University of Nottingham, University Park, Nottingham NG7 2RD, United Kingdom

⁵ Institut d’Astrophysique de Paris, UMR 7095, CNRS and Sorbonne Université, 98 bis boulevard Arago, 75014 Paris, France

⁶ SISSA - Scuola Internazionale Superiore di Studi Avanzati, Via Bonomea 265, 34136 Trieste, Italy and INFN Sezione di Trieste

⁷ IFPU - Institute for Fundamental Physics of the Universe, Via Beirut 2, 34014 Trieste, Italy

⁸ Université Paris Cité, CNRS, Astroparticule et Cosmologie, F-75013 Paris, France

⁹ Department of Astrophysical Sciences, Princeton University, Princeton, NJ 08544, USA

November 20, 2024

ABSTRACT

Aims. We develop a parametrised model to describe the formation and evolution of massive black holes, designed for comparisons with both electromagnetic and gravitational wave observations.

Methods. Using an extended Press-Schechter formalism, we generate dark matter halo merger trees. We then seed and evolve massive black holes through parameterised prescriptions. This approach, which avoids solving differential equations, is computationally efficient, enabling us to analyse observational data and infer the parameters of our model in a fully Bayesian framework.

Results. We find that observations of the black hole luminosity function are compatible with the nHz gravitational wave signal (likely) measured by pulsar timing arrays (PTAs), provided we allow for an increased luminosity function at high redshift ($4 - 7$), as recently suggested by JWST observations. Our model can simultaneously reproduce the bulk of the $M_* - M_{\text{BH}}$ relation at $z = 0$, as well as its outliers, something cosmological simulations struggle to do. The inferred model parameters are consistent with expectations from observations and more complex simulations: They favour heavier black hole seeds and short delays between halo and black hole mergers, while requiring super-Eddington accretion episodes lasting a few tens of million years, which in our model are linked to galaxy mergers. We find accretion to be suppressed in the most massive black holes below $z \approx 2.5$, consistently with the anti-hierarchical growth hypothesis. Finally, our predictions for LISA, although fairly broad, are in agreement with previous models that assumed efficient merging of massive black holes formed from heavy seeds.

Conclusions. Our model offers a new perspective on the apparent tensions between the black hole luminosity function and the latest JWST and PTA results. Its flexibility makes it ideal to fully exploit the potential of future gravitational wave observations of massive black hole binaries with LISA.

1. Introduction

Massive black holes (MBHs), with masses of $10^5 - 10^9 M_\odot$, reside at the centre of most galaxies in our local Universe (Gehren et al. 1984; Kormendy & Richstone 1995; Reines et al. 2011; Reines et al. 2013; Baldassare et al. 2020), including our own Milky Way. These cosmic giants play a crucial role in the evolution and dynamics of galaxies, as demonstrated by numerous scaling relations between the properties of galaxies and their MBHs (Ferrarese & Merritt 2000; Tremaine et al. 2002; Kormendy & Ho 2013; McConnell & Ma 2013; Schramm & Silverman 2013; Scott et al. 2013; Shankar 2013; Shankar et al. 2019; Sahu et al. 2019; Greene et al. 2020), such as the $M_* - M_{\text{BH}}$ relation with the stellar mass of the host galaxy. Such linked properties point to the fact that MBHs track the hierarchical formation of galaxies, and possibly at the mutual influence between MBHs and galaxies. However, the details of the processes governing the origin, growth, activity, and feedback of these black holes (BHs) remain highly debated.

The general picture can be sketched as follows. MBHs must have originated at high redshift from lighter black hole “seeds”. Several seed models have been proposed, ranging from “light” to “heavy” (for a review, see Latif & Ferrara 2016; Volonteri et al. 2021). At the largest scales, the fate of a seed will be determined by the evolution of its host dark matter halo, which proceeds hierarchically in mass. Within the host galaxy, the growth of the seed proceeds primarily through the accretion of gas (Yu & Tremaine 2002), and in minor part via the accretion of stars (Rees 1988), with periods of intense accretion activity likely alternated by quiescent phases. Intense accretion emits significant energy, in a variety of forms: radiation is emitted across the electromagnetic spectrum (Fabian 2012), while kinetic and thermal energy can affect gas temperature, density and turbulence, and in turn prevent new gas from reaching the MBH and temporarily suppress the process (AGN feedback). Although to a lesser extent (Ricarte et al. 2019), BH mergers following the merger of their host galaxies can also contribute to the growth of MBHs (Dubois et al. 2014; Kulier et al. 2015).

One of our best probes of the population of MBHs is the luminosity function (LF) of accreting MBHs: quasars and active galactic nuclei (AGNs) more generally. This has been the target of surveys in the X-ray, UV, optical, infrared, and radio bands (see Hopkins et al. 2007; Shen et al. 2020, and references therein). These surveys, covering out to $z \lesssim 7$, have revealed that the LF evolves strongly – in normalisation and shape – with redshift. Interestingly, mid-infrared surveys appeared in tension with the aforementioned results. Using observations from the Spitzer Space Telescope survey (Werner et al. 2004), Lacy et al. (2015) found an increased LF up to $z \sim 3$. The higher redshift mid-infrared Universe is now being probed by the James Webb Space Telescope (JWST) (Gardner et al. 2006). It has detected tens of candidate AGNs at high redshift ($z \sim 4-11$), including some at lower bolometric luminosities than those observed so far ($L_{\text{bol}} \sim 10^{44} - 10^{46} \text{ erg/s}$) (e.g., Onoue et al. 2023; Kocevski et al. 2023; Maiolino et al. 2023; Kokorev et al. 2023; Lyu et al. 2024). The first results for the LF and mass function derived from these observations (Harikane et al. 2023; Maiolino et al. 2023; Greene et al. 2024; Matthee et al. 2024; Taylor et al. 2024) also point to an increased LF compared to previous expectations – based on the compilation of data from mid-IR to X-ray, but dominated at high redshift by X-ray and UV observations (Shen et al. 2020). It has been suggested that the masses and abundance of (candidate) MBHs found by JWST at very high redshifts might pose a challenge for lighter seed scenarios, and might require continuous and intense accretion even for heavier seeds (e.g., Harikane et al. 2023; Maiolino et al. 2023; Kokorev et al. 2023; Greene et al. 2024). At the same time, the models producing the heaviest seeds appear to struggle to produce enough seeds to explain the abundance of (candidate) MBHs (Regan & Volonteri 2024). See also Habouzit (2024) for a discussion on the compatibility of different simulations of MBH evolution with these results.

These electromagnetic observations are now being complemented with gravitational wave (GW) observations, as Pulsar Timing Array (PTA) collaborations are likely close to confirming the detection of a stochastic background consistent with merging MBH binaries with masses $\gtrsim 10^8 M_{\odot}$ (Antoniadis et al. 2023c; Agazie et al. 2023b; Tarafdar et al. 2022; Reardon et al. 2023; Xu et al. 2023). It is generally believed that the preliminary result for the PTA background, with its relatively high amplitude, would require MBHs to merge and accrete efficiently (Agazie et al. 2023a; Antoniadis et al. 2024; Barausse et al. 2023; Izquierdo-Villalba et al. 2024), although see Goncharov et al. (2024). In the next decade, the Laser Interferometer Space Antenna (LISA) will further extend our understanding of merging MBHs by detecting GWs from binaries with lower masses ($10^4-10^8 M_{\odot}$) and up to very high redshifts ($z \sim 20$) (Amaro-Seoane et al. 2017; Colpi et al. 2024).

The astrophysical interpretation of observations is achieved by comparing to theoretical models for the formation and evolution of MBHs. Cosmological N -body and hydrodynamic simulations have become valuable tools for simulating MBHs, thanks to increased computational power and more accurate sub-grid models for MBH accretion, seeding, feedback and dynamics: see, e.g., Volonteri et al. (2016); Springel et al. (2017); Kannan et al. (2021); Ni et al. (2022); Bhowmick et al. (2024). In addition to those, semi-analytical models (SAMs; e.g., Cole et al. 2002; Volonteri et al. 2003; Monaco et al. 2007; Somerville et al. 2008; Benson 2012; Barausse 2012; Ricarte & Natarajan 2018; Bonetti et al. 2019; Dayal et al. 2019; Izquierdo-Villalba et al. 2020; Barausse et al. 2020; Trinca et al. 2022) have been widely used to simulate the cosmic history of MBHs thanks to their reduced computational cost. A computationally cheaper alterna-

tive to both SAMs and cosmological simulations are empirical models (see, e.g., Soltan 1982; Small & Blandford 1992; Tucci & Volonteri 2017; Conroy & White 2012; Allevato et al. 2021). Rather than making physical assumptions, these models use observations to empirically (and self-consistently) characterise the evolution of MBHs. Empirical models have grown more and more complex, with some (Zhang et al. 2023; Boettner et al. 2023) encompassing dark matter halos, galaxies and MBHs and counting around 50 parameters. The more complex the model, the more observations must be used to constrain its parameters, from scaling relations to luminosity and mass functions.

Cosmological simulations and SAMs are too computationally expensive to compare the full range of alternative models and parameter space with observations, resulting in a set of discrete models. This is a major obstacle for astrophysical inference within a Bayesian framework. In Toubiana et al. (2021), some of the present authors carried out a study of mock LISA data and showed that inference with a finite set of discrete population models could lead to severe biases in the underlying astrophysical parameters. Empirical models, while sufficiently fast for Bayesian parameter estimation (see, e.g., Zhang et al. 2023; Boettner et al. 2023), focus on statistical and empirical properties, rather than the underlying physics.

The goal of this work is to provide a *fast* parametric approach to infer the physics behind the evolution of MBHs from current observations, and prepare for the LISA mission. We introduce our model POMPOCO: *Parametrisation Of the Massive black hole POpulation for Comparison to Observations*. It adopts an intermediate approach between SAMs and empirical models, proposing an effective description of the formation and evolution of MBHs within their host halos. The backbone of our model is a dark matter (DM) halo merger tree, which we generate and then populate with MBHs which are seeded – starting from high redshifts $z \geq 10$ – accrete and merge according to parametric prescriptions. Replacing the physics-informed semi-analytic prescriptions entering SAMs with this effective description allows for a significant computational speed-up. Thus, we can assign the 12 parameters entering our model large priors, rather than making narrow or discrete choices based on (uncertain) physical models, as in traditional SAMs. We then explore the parameter space using a Markov-Chain-Monte-Carlo (MCMC) algorithm to find the sets of parameters that are compatible with the desired datasets.

As a first application of POMPOCO, we jointly fit the LF at low and high redshifts and the amplitude of the GW background measured by PTA. We find that by allowing for an increased LF at high redshift, as hinted by an extrapolation of Lacy et al. (2015) and now direct observations with JWST (Harikane et al. 2023; Maiolino et al. 2023; Greene et al. 2024; Matthee et al. 2024; Taylor et al. 2024), we can consistently describe these observations. We find a small preference for a slightly lower GW background, but still compatible with current PTA results. We cross-check our results through the $M_{*} - M_{\text{BH}}$ relation at $z = 0$, for which we do not explicitly fit, and find a good agreement with the proposed fit of Greene et al. (2020). Moreover, we are also able to produce some of the observed BHs that are not in the bulk of the distribution, a challenge for many models (Habouzit et al. 2021). We obtain the posterior distribution for the parameters of POMPOCO. The inferred model parameters align well with both observational data and more comprehensive numerical simulations. They support a scenario in which massive black holes form from heavy seeds, with relatively short delays between halo and black hole mergers, extending just beyond the timescale for dynamical friction. Additionally, the model suggests that super-

Eddington accretion, in burst episodes lasting a few tens of million years, is important for BH evolution. We have assumed for simplicity that such episodes occur following galaxy mergers, although super-Eddington episodes may also be triggered by in-situ accretion of dense gas clouds (Lupi et al. 2016; Sassano et al. 2023; Lupi et al. 2024). Our results indicate that accretion is suppressed for the most massive black holes starting around a redshift of 2.5, reinforcing the notion of anti-hierarchical growth in these systems. Lastly, while our predictions for LISA are fairly broad, they remain consistent with previous models proposing efficient mergers of massive black holes originating from heavy seeds.

This paper is organised as follows. Section 2 describes our parametric model. In Sec. 3 and 4 we describe how we construct observables from our model, and use them to fit the model parameters to observations. We present our results in Sec. 5, and make predictions for the LISA mission in Sec. 6. We summarise and conclude in Sec. 7. In the remaining of the paper, MBH masses are defined in the source frame.

2. Description of the model

We describe the components of our model below. We also summarise all the parameters and the settings of our model in Table 1. In the current version of our model, we do not track the evolution of the spins of massive BHs. We hope to include BH spins in future work. We adopt a flat Λ CDM cosmology with $H_0 = 67.77 \text{ km s}^{-1} \text{ Mpc}^{-1}$, $\Omega_m = 0.3071$, $\Omega_b = 0.04820$ and $\delta_{c,0} = 1.686$ for the critical overdensity for spherical collapse at $z = 0$. Given the tight constraints on cosmological parameters, we expect the uncertainty from cosmology to be small compared to the astrophysical uncertainty.

2.1. Dark matter halo merger tree

We generate DM halo merger trees down to $z_{\text{max}} = 20$ using the implementation of the extended Press-Schechter formalism (Press & Schechter 1974; Bond et al. 1991; Bower 1991; Lacey & Cole 1993) described in App. A of Parkinson et al. (2008). We use updated values given in Benson (2017) for the phenomenological modifications to the original extended Press-Schechter formalism, introduced to better reproduce cosmological simulations. We use a time-varying mass resolution, as proposed in Volonteri et al. (2003): $M_{h,\text{res}} = 10^{-3} M_{h,0} (1+z)^{-3.5}$, where $M_{h,0}$ is the mass of the halo at $z = 0$.

The suite of trees is built drawing the halo masses at $z = 0$ from a log-uniform distribution. Each tree will enter the calculation of population properties by reweighting the BHs in that tree by their Press-Schechter weight.

2.2. Massive black hole seeds

We populate leaf halos – the last halos along the branches of the merger trees¹ – with seed BHs. We only seed halos at $z \geq 10$ and with mass above a threshold $M_{h,\text{seed}}$, with probability f_{seed} .

The nature and mass spectrum of the original seeds of the observed population of MBHs is currently unconstrained. Proposed seeding mechanisms range from light seeds (below $10^3 M_\odot$), resulting from the first stars or formed primordially, and heavy seeds (between $10^3 M_\odot$ and $10^6 M_\odot$) resulting from runaway accretion, mergers or supermassive stars. For a recent review of

¹ Leaf halos can be at $z < z_{\text{max}}$, if their mass drops below the mass resolution.

these mechanisms, which are not mutually exclusive, see Volonteri et al. (2021). We allow our model to probe the seed distribution by drawing the mass of the seed BH from a truncated log-normal distribution, with mean μ_{seed} and standard deviation σ_{seed} . At the high end, we limit the mass of the BH seed to 10% of the baryonic mass of the halo $M_h \Omega_b / (\Omega_m - \Omega_b)$. At the low end, we take the minimum seed mass to be $100 M_\odot$.² We denote the seeded BH as *primary* BH of the DM halo.

2.3. Halo and massive black hole mergers

Following the merger of two halos, we track the evolution of the BHs they contain, distinguishing between *major* and *minor* halo mergers, based on the halo mass ratio $q_h = M_{h,2}/M_{h,1} \leq 1$. Based on the results of our simulations, we set the threshold for major mergers to $q_{h,\text{major}} = 0.13$, which is similar to the value used in Ricarte & Natarajan (2018).

2.3.1. Formation of black hole binaries

Following major mergers, where $q_h \geq q_{h,\text{major}}$, we check whether either halo hosts a BH. If there is only one BH, this becomes the primary BH of the newly formed halo. If there is one BH in each, they form a binary with merger time given by the sum of the dynamical friction (DF) timescale and additional delays (see Sec. 2.3.3). Finally, if there are more BHs, we use the prescription for multiple interactions described below.

In the case of minor mergers, BHs in the lighter halo have to sink into the heavier halo before being counted as primary BH or forming a binary. The BHs of the lighter halo are therefore dubbed as *outer* BHs of the heavier halo. The sinking time is given by the DF timescale of the satellite halo into the primary one. If the lighter halo contains a binary that merges before the sinking time, we allow it to merge and assign the merger product to the new halo as an outer BH. We retain (the most massive) half of the outer BHs of the lighter halo, in addition to its potential primary/binary, up to a limit of four outer BHs. We find that this is an acceptable limitation, as small BHs in small halos play a minor role. Similarly, following major mergers, we retain up to four of the outer BHs of the two halos, selecting the ones with the shorter sinking times. When outer BHs sink into the centre of the halo, they either become the primary BH of that halo if it contained none, or form a binary that merges within t_{delay} (see Sec. 2.3.3). If the halo already contained a binary, or multiple outer BHs sink within one time step, we use our prescription for multiple interactions described in Sec. 2.3.2.

2.3.2. Multiple interactions

We use the results of Bonetti et al. (2018a) to handle interactions between more than two BHs. We decide with probability $p_{\text{multi}} = 0.22$ if the BHs undergo a multiple interaction or not (see Table 2 of Bonetti et al. (2018a)). If it occurs, we retain the two most massive BHs and draw the merger time (in yr) from a log-normal distribution with mean 8.4 dex and standard deviation 0.4 dex (see Fig. 7 of Bonetti et al. (2018a)). If they do not undergo a multiple interaction, we distinguish between two cases, depending on how the BHs "met". If there was a binary and a third BH was brought either by a halo merger or by an outer BH that sunk, we keep the original binary. If there was

² We exclude stellar-mass seeds below $m < 100 M_\odot$, as Refs. Smith et al. (2018), Shi et al. (2024) found that less than a percent can grow to contribute to the MBH population.

no binary originally, e.g. there was a primary BH and 2 outer BHs sink within one time step, we just keep the two most massive among them, and form a binary merging within t_{delay} (see Sec. 2.3.3). In any case, we do not keep track of the other BHs.

2.3.3. Dynamical friction and other delays

Satellite halos (and their BHs) sink to the centre of the primary halo via DF, whose typical timescale is set by (Lacey & Cole 1993; Binney & Tremaine 1987)

$$t_{\text{DF}} = 0.495 \frac{1 + q_h}{q_h} \frac{1}{H(z) \sqrt{\Delta_{\text{vir}}} \ln(1 + q_h)}, \quad (1)$$

$$\Delta_{\text{vir}} = 178 \Omega_m(z)^{0.45}, \quad (2)$$

$$q_h = \frac{M_{h,2}}{M_{h,1}}, \quad (3)$$

where we made the same choice for the numerical prefactor as in Volonteri et al. (2003), and where $H(z)$ is the Hubble factor at the desired redshift. We neglect any possible variations in the DF timescale due to the initial conditions of the infall, and effects such as tidal stripping and tidal heating of the satellite halo.

Once the satellite halo has sunk into the primary one, the two galaxies they host will merge thanks to additional DF. The BHs at their center will then form a bound binary, with separation of order of a parsec. The binary will undergo several other processes that affect its orbital decay, including stellar hardening and interactions with nuclear gas (see Colpi 2014, for a review). We model these additional delays with a single parameter, t_{delay} , taken to be the same for all binaries. Our model could be extended by allowing the delay time to be drawn from a parametrised distribution depending on the physical parameters of the system.

2.3.4. Merger

Once the total time delay has elapsed, binaries merge and form remnants with mass given by the sum of the masses at the time of the merger. We neglect the mass loss due to the emission of GWs, but we do account for the accretion occurring from binary formation until merger, using the prescriptions described in the section below. We label the merger remnant as the primary BH of its host halo.

We do not model kicks on the remnant BH due to the emission of GWs, which could displace the BH from the centre of its host, because they depend sensitively on the BH spins and the details of the orbit at the time of merger (eccentricity, spin inclinations), which we do not track in the current version of POMPOCO. Kicks are expected to have a small impact in high-mass galaxies, because of their large escape velocity. Those are the galaxies that contribute the most to the GW background in the nHz band and the high end of the LF, which are the observables of interest for this paper. Thus, neglecting kicks should have little impact on our results. However, it could impact the LISA rates, since many LISA mergers occur in low-mass galaxies, and could modify the low mass end of the M_* - M_{BH} relation. We leave the inclusion of kicks for future work.

2.4. Accretion

We parametrise the growth of the mass of a BH, m_{BH} , through accretion by the Eddington ratio, f_{Edd} ,

$$\dot{m}_{\text{acc}} = f_{\text{Edd}} \dot{m}_{\text{Edd}}, \quad (4)$$

$$\dot{m}_{\text{BH}} = (1 - \epsilon) \dot{m}_{\text{acc}}, \quad (5)$$

$$\dot{m}_{\text{Edd}} = \frac{m_{\text{BH}}}{\epsilon t_{\text{Edd}}} = \frac{L_{\text{Edd}}}{\epsilon c^2}, \quad (6)$$

where \dot{m}_{Edd} and L_{Edd} are the Eddington accretion rate and luminosity, respectively, ϵ is the radiative efficiency, and $t_{\text{Edd}} = 450$ Myr defines the accretion timescale. Thus, between two time steps, the mass increases as

$$m_{\text{BH}}(t + \Delta t) = m_{\text{BH}}(t) \exp\left(f_{\text{Edd}} \frac{1 - \epsilon}{\epsilon} \frac{\Delta t}{t_{\text{Edd}}}\right). \quad (7)$$

We take the radiative efficiency to be 0.1. Inspired by Ricarte & Natarajan (2018), we consider two accretion modes: *burst* and *steady* accretion.

The burst mode is triggered following a major halo merger, $q_h \geq q_{h,\text{major}}$. Such mergers are expected to feed the reservoir surrounding MBHs, leading to an episode of intense accretion. When this happens, the most massive BH in the resulting galaxy starts accreting for a time t_{burst} with an Eddington ratio $f_{\text{Edd,burst}}$. In the burst mode, we do allow for super-Eddington accretion, and draw $f_{\text{Edd,burst}}$ from a power-law distribution with slope $(\gamma_{\text{burst}} - 1)$ between 10^{-2} and 10. In this work, we consider a common burst time t_{burst} for all BHs. If the resulting halo undergoes another major merger before a time t_{burst} has elapsed, we restart the count.

Whenever they are not accreting in the burst mode, BHs accrete in the steady mode with an Eddington ratio $f_{\text{Edd,steady}}$ drawn from a log-normal distribution with mean μ_{steady} and variance σ_{steady} truncated at the high end at 1. When drawing $f_{\text{Edd,steady}}$, we draw jointly t_{steady} from a log-uniform distribution between 1 and 100 Myr. After a time t_{steady} has elapsed, we draw again both quantities. This procedure is meant to capture the variability of AGNs.

The most massive BHs are observed to be quiescent at low redshift due to gas having been consumed by star formation, as well as affected by supernova and AGN feedback (see Merloni 2004; Hirschmann et al. 2012, 2014, and references therein). To reproduce this, for $z \leq z_{\text{cut}}$ we shut off accretion for BHs with $m_{\text{MBH}} \geq m_{\text{cut}}(z)$. We parametrise $m_{\text{cut}}(z)$ as

$$\log_{10} m_{\text{cut}}(z) = \log_{10} m_{\text{cut},0} (1 + z)^{\alpha_{\text{cut}}}, \quad (8)$$

where $\log_{10} m_{\text{cut},0}$ and α_{cut} are parameters of our model, together with z_{cut} . We impose $\alpha_{\text{cut}} \geq 0$ so that the mass cut is larger at higher redshift. This approach gives our model the flexibility to capture the anti-hierarchical growth observed in data and simulations (Merloni 2004; Hirschmann et al. 2012, 2014), without enforcing it a priori³.

We apply the prescriptions above to the primary and binary BHs of all halos. Outer BHs do not accrete in our model, as we do not expect them to have a sufficient reservoir to accrete significantly. Both BHs in a binary have the same f_{Edd} (either burst or steady).

³ For instance, if the posterior of z_{cut} was to favour values close to 0, or the one of $m_{\text{cut},0}$ values above the mass of most astrophysical BHs, e.g. $10^{11} M_{\odot}$, this would be a sign that the model does not need anti-hierarchical growth to fit the data.

Parameter	Description	Prior/Value
$M_{h,\text{seed}} [M_{\odot}]$	minimum mass of the halos that host a seed BH	$\log \mathcal{U}[10^6, 10^{7.7}]$
f_{seed}	probability to seed a leaf halo with $M_h \geq M_{h,\text{seed}}$ at $z \geq 10$	$\log \mathcal{U}[0.01, 1]$
$\mu_{\text{seed}} [M_{\odot}]$	mean of the log-normal distribution of seed masses	$\log \mathcal{U}[10^{2.5}, 10^6]$
$\sigma_{\text{seed}} [\text{dex}]$	standard deviation of the log-normal distribution of seed masses	$\log \mathcal{U}[10^{0.5}, 10^2]$
$t_{\text{delay}} [\text{Myr}]$	additional time delay (after DF timescale) for BH binary merger	$\log \mathcal{U}[10^{-0.5}, 10^4]$
$t_{\text{burst}} [\text{Myr}]$	duration of burst accretion mode	$\log \mathcal{U}[1, 100]$
γ_{burst}	slope of the power-law distribution of $f_{\text{Edd,burst}}$	$\mathcal{U}[-1, 0]$
$\mu_{\text{steady}} [\text{dex}]$	mean of the log-normal distribution of $f_{\text{Edd,steady}}$	$\mathcal{U}[-6, -3]$
$\sigma_{\text{steady}} [\text{dex}]$	standard deviation of the log-normal distribution of $f_{\text{Edd,steady}}$	$\mathcal{U}[0.5, 3]$
z_{cut}	redshift below which accretion is cut in the most massive BHs	$\mathcal{U}[1, 4]$
$m_{\text{cut},0} [M_{\odot}]$	mass at $z = 0$ above which accretion is cut	$\log \mathcal{U}[10^6, 10^{7.3}]$
α_{cut}	slope of the increase in the mass cut for accretion with redshift, see Eq. (8)	$\mathcal{U}[0, 0.5]$
$f_{\text{Edd,burst}}$	burst mode Eddington ratio	$\mathcal{PL}(\gamma_{\text{burst}} - 1, 10^{-2}, 10)$
$f_{\text{Edd,steady}}$	steady mode Eddington ratio	$\log \mathcal{N}(\mu_{\text{steady}}, \sigma_{\text{steady}}) \leq 1$
$t_{\text{steady}} [\text{Myr}]$	duration of a steady accretion episode, after which $f_{\text{Edd,steady}}, t_{\text{steady}}$ are redrawn	$\log \mathcal{U}[1, 100]$
ϵ	radiative efficiency	0.1
$q_{h,\text{major}}$	mass ratio threshold for major halo mergers	0.13
p_{multi}	probability of interaction between three or more BHs	0.22

Table 1. Parameters and settings of our model. The first 12 lines (before the double bar) list the free parameters of our model, which we fit to observations. The remaining lines summarise the distributions on quantities entering the simulations and the parameters that are fixed in our model. In the third column, $(\log) \mathcal{U}$ stands for a (log-) uniform distribution in the given range, \mathcal{PL} for a power-law distribution with given slope and range and $\log \mathcal{N}$ for a log-normal distribution with given mean and standard deviation.

3. Observables

To simulate the population of MBHs in the Universe for a given choice of parameters, we apply the following procedure:

- We build N_h merger trees, drawing the mass of the halos at $z = 0$ from a log-normal distribution between 10^{11} and $10^{15} M_{\odot}$;
- We populate each merger tree according to the model parameters;
- We save the properties of the BHs in the merger tree (mass, Eddington ratio, mass of the host halo, etc.) at a set of redshifts.

In this work, we generate $N_h = 2000$ halos.

The generation of the DM halo merger tree is the most time-consuming step of our model. Fortunately, none of the parameters affect this step. Therefore, we can generate a single merger tree and run simulations for any number of parameters on it. This results in a relatively fast model, and allows us to thoroughly explore the parameter space. As an example, it takes ~ 1 hour to generate a merger tree and run the simulation for 500 sets of parameters on it. The 2000 merger trees are run in parallel and the results are combined in post-processing.

We will now describe how to transform the output of our simulations into quantities that can be compared with observations: the LF, the stellar mass-black hole mass relation, the stochastic GW background, and the merger rate.

3.1. Luminosity function

The luminosity of a BH is given by

$$L_{\text{BH}} = f_{\text{Edd}} \frac{m_{\text{BH}}}{t_{\text{Edd}}} c^2, \quad (9)$$

where f_{Edd} is either the burst mode or steady mode Eddington ratio, depending on the current accretion mode of the BH. We assign binaries a luminosity equal to the sum of the luminosities of the individual BHs (recall that in our model, BHs in a binary share the same f_{Edd}). Outer BHs of a halo are not included in the computation of the LF since we do not expect them to accrete significantly.

We denote the LF at redshift z_0 by $\Phi(L_{\text{BH}}, z_0)$. It is given by the weighted sum of the contribution from each halo merger tree,

$$\Phi(L_{\text{BH}}, z_0) = \int W_{\text{PS}}(M_{h,0}) \frac{dN_{M_{h,0}}}{d \log_{10} L_{\text{BH}}} \Big|_{z_0} dM_{h,0}, \quad (10)$$

where $W_{\text{PS}}(M_{h,0})$ is the Press-Schechter weight for a halo of mass $M_{h,0}$ at $z = 0$ and $\frac{dN_{M_{h,0}}}{d \log_{10} L_{\text{BH}}} \Big|_{z_0}$ is the number of BHs with luminosity L_{BH} at redshift z_0 in the merger history of a halo of mass $M_{h,0}$ at $z = 0$. We compute the integral in a discrete way, by the PS-weighted sum of the individuals histograms of each tree. Binning in log-luminosity, we have for the LF in bin k

$$\Phi(L_{\text{BH},k}, z_0) = \frac{\mathcal{D}_h}{N_h \Delta_{L_{\text{BH}}}} \sum_i W_{\text{PS}}(M_{h,0,i}) \frac{dN_i}{d \log_{10} L_{\text{BH},k}} \Big|_{z_0}, \quad (11)$$

with $\Delta_{L_{\text{BH}}}$ the size of the bin in $\log_{10} L_{\text{BH}}$ and $\mathcal{D}_h = \log_{10}(M_{h,0,\text{max}}) - \log_{10}(M_{h,0,\text{min}})$ coming from the normalisation of the log-uniform distribution used to draw the halo masses. The Poisson error in each bin is obtained by assuming that the histograms resulting from the different simulations are independent Poisson realisations. Thus, the variances sum up and the error is

given by

$$\Delta\Phi(L_{\text{BH},k}, z_0) = \frac{\mathcal{D}_h}{N_h \Delta L_{\text{BH}}} \sqrt{\sum_i W_{\text{PS}}(M_{h,0,i})^2 \frac{dN_i}{d \log_{10} L_{\text{BH},k}} \Big|_{z_0}}. \quad (12)$$

3.2. Stellar mass-black hole mass relation

In our code, we do not directly model the evolution of the stellar mass M_* of a given halo. Rather, we use the halo mass-stellar mass relation of [Moster et al. \(2010\)](#) to convert M_h into M_* , including the scatter in the relation, to account for the spread in the relation.

For a given stellar mass at redshift z_0 , we can compute the average black hole mass across halos at that redshift as

$$M_{\text{BH}}(M_*, z_0) = \frac{\int W_{\text{PS}}(M_{h,0}) \frac{dN_{M_{h,0}}}{dm_{\text{BH}} dM_*} \Big|_{z_0} m_{\text{BH}} dm_{\text{BH}} dM_{h,0}}{\int W_{\text{PS}}(M_{h,0}) \frac{dN_{M_{h,0}}}{dM_*} \Big|_{z_0} dM_{h,0}}, \quad (13)$$

where $\frac{dN_{M_{h,0}}}{dm_{\text{BH}} dM_*} \Big|_{z_0}$ is the number of halos at redshift z_0 that contain a BH with mass m_{BH} and whose stellar mass is M_* , in the merger history of a halo of mass $M_{h,0}$ at $z = 0$.

In practice, we predefine a fixed binning scheme for the stellar masses, and then associate each halo hosting a BH to the corresponding $M_{*,k}$ bin based on the $M_h - M_*$ relation of [Moster et al. \(2010\)](#). We have

$$M_{\text{BH}}(M_{*,k}, z_0) = \frac{\sum_i W_{\text{PS}}(M_{h,0,i}) \sum_j m_{\text{BH},i,j,k}}{\sum_i W_{\text{PS}}(M_{h,0,i}) N_{i,k}}, \quad (14)$$

where $m_{\text{BH},i,j,k}$ are the masses of the BHs in halos at z_0 in the i -th simulation whose stellar mass is in the $M_{*,k}$ bin, and $N_{i,k}$ is the number of such halos. In the case of binaries, we use the total mass. Outer BHs are not included in this computation.

We compute the standard deviation of the $M_{\text{BH}} - M_*$ relation as

$$\Delta M_{\text{BH}}(M_{*,k}, z_0) = \sqrt{\frac{\sum_i W_{\text{PS}}(M_{h,0,i}) \sum_j m_{\text{BH},i,j,k}^2}{\sum_i W_{\text{PS}}(M_{h,0,i}) N_{i,k}} - M_{\text{BH}}(M_{*,k}, z_0)^2}. \quad (15)$$

Technically, there should also be a Poisson error (on N_i), but we neglect it, as we take the bins in stellar mass to be big enough so that the dominant source of error is the variance of BH masses within that bin and not the counting.

3.3. Stochastic gravitational wave background

We compute the stochastic GW signal in the PTA band of our simulations with the formalism of [Phinney \(2001\)](#) and [Sesana et al. \(2008\)](#). In this work, we assume binaries to be on quasi-circular orbits. We introduce the chirp mass of a binary with masses m_1 and m_2 as $\mathcal{M}_c = (m_1^3 m_2^3)/(m_1 + m_2)^5$. Denoting the characteristic GW amplitude at (observer) frequency f as $h_c(f)$, we have

$$h_c^2(f) = \frac{4G}{\pi f^2 c^2} \int \frac{W_{\text{PS}}(M_{h,0})}{1+z} \frac{dN_{M_{h,0}}}{d\mathcal{M}_c dz} \frac{dE_{\text{GW}}(\mathcal{M}_c)}{d \ln f_r} dz d\mathcal{M}_c dM_{h,0}, \quad (16)$$

where $\frac{dN_{M_{h,0}}}{d\mathcal{M}_c dz}$ is the number of halos hosting a binary merger with chirp mass \mathcal{M}_c at redshift z in the merger history of a halo of

mass $M_{h,0}$ at $z = 0$, and $\frac{dE_{\text{GW}}(\mathcal{M}_c)}{d \ln f_r}$ is the energy emitted in the source rest-frame at frequency $f_r = f(1+z)$. For quasi-circular binaries, the latter is given by

$$\frac{dE_{\text{GW}}(\mathcal{M}_c)}{d \ln f_r} = \frac{(\pi \mathcal{M}_c G f_r)^{2/3}}{3} \mathcal{M}_c. \quad (17)$$

Thus, the characteristic strain has a power-law frequency dependence

$$h_c^2(f) = \frac{4G^{5/3}}{3\pi^{1/3} c^2} f^{-4/3} \int W_{\text{PS}}(M_{h,0}) \frac{dN_{M_{h,0}}}{d\mathcal{M}_c dz} \frac{\mathcal{M}_c^{5/3}}{(1+z)^{1/3}} dz d\mathcal{M}_c dM_{h,0}. \quad (18)$$

with the amplitude determined by the distribution of mergers in a given simulation. In practice, we perform a Monte-Carlo integration,

$$h_c^2(f) = \frac{4G^{5/3} \mathcal{D}_h}{3\pi^{1/3} c^2} f^{-4/3} \sum_i W_{\text{PS}}(M_{h,0,i}) \sum_j \frac{\mathcal{M}_{c,i,j}^{5/3}}{(1+z_{i,j})^{1/3}}, \quad (19)$$

where the second sum is performed over all the mergers in the i -th merger tree. The Poisson error is then given by

$$\Delta h_c^2(f) = \frac{4G^{5/3} \mathcal{D}_h}{3\pi^{1/3} c^2} f^{-4/3} \sqrt{\sum_i W_{\text{PS}}(M_{h,0,i})^2 \sum_j \left(\frac{\mathcal{M}_{c,i,j}^{5/3}}{(1+z_{i,j})^{1/3}} \right)^2}. \quad (20)$$

Finally, following [Antoniadis et al. \(2024\)](#), we define the root-mean-square residual as

$$\rho_c^2(f) = \frac{h_c^2(f)}{12\pi^2 f^3} \Delta_f, \quad (21)$$

where Δ_f is the frequency resolution (the inverse of the observation time).

3.4. Merger rate

We introduce $m_t = m_1 + m_2$ as the total mass of an MBH binary and $q_b = m_1/m_2 \geq 1$ its mass ratio. The rate of MBH mergers per unit m_t , q_b and z is computed as

$$\frac{dN}{dt dm_t dq_b dz} = \int 4\pi d_c(z)^2 c W_{\text{PS}}(M_{h,0}) \frac{dN_{M_{h,0}}}{dm_t dq_b dz} dM_{h,0}, \quad (22)$$

where $d_c(z)$ is the comoving distance at redshift z and $\frac{dN_{M_{h,0}}}{dm_t dq_b dz}$ is the number of MBH mergers with parameters (m_t, q_b, z) in the merger history of a halo of mass $M_{h,0}$ at $z = 0$, t is the detector-frame time. Monte-Carlo integration gives

$$\frac{dN}{dt dm_t dq_b dz} = \frac{\mathcal{D}_h}{N_h} \sum_i 4\pi d_c(z)^2 c W_{\text{PS}}(M_{h,0,i}) \frac{dN_i}{dm_t dq_b dz}. \quad (23)$$

In practice, to generate samples of observed MBH merger events for an observation time T_{obs} we use the following procedure. We read the (m_t, q_b, z) values of all merger events in our trees, attribute them a Poisson rate

$$\lambda(m_t, q_b, z) = \frac{4\pi d_c(z)^2 c W_{\text{PS}}(M_{h,0,i}) \mathcal{D}_h}{N_h}, \quad (24)$$

and draw the number of such events from a Poisson distribution with expected number $\lambda(m_t, q_b, z) T_{\text{obs}}$.

The detector-frame rate as a function of a single parameter, e.g. m_t , is obtained by marginalising over the remaining parameters, and the total rate is obtained by marginalising over all parameters (m_t, q_b, z)

$$\frac{dN}{dt} = \int 4\pi d_c(z)^2 c W_{\text{PS}}(M_{h,0}) \frac{dN_{M_{h,0}}}{dm_t dq_b dz} dM_{h,0} dm_t dq_b dz, \quad (25)$$

see also Eq. (2) of Hartwig (2019). Finally, Monte-Carlo integration gives

$$\frac{dN}{dt} = \sum_{(m_t, q_b, z)} \lambda(m_t, q_b, z). \quad (26)$$

4. Fitting to observations

As a first application of POMPOCO, we fit jointly the LF across redshifts and the GW stochastic background.

4.1. Observations

As the observed LF, we consider a combination of the fits from Lacy et al. (2015) (fit: ‘All’) and Shen et al. (2020) (fit: ‘global A’), as described in the next section (Fig. 1). The fit by Shen et al. (2020) is based on a wide range of observations in the rest-frame mid-IR, B band, UV, soft and hard X-ray going up to $z \sim 7$. The constraint by Lacy et al. (2015) is only based on the mid-IR Spitzer Space Telescope survey with observations up to $z \sim 3$. It is also included in the compilation of Shen et al. (2020), although the latter is mainly driven by the more abundant B, UV, and X-ray data. The mid-IR LF fit in Lacy et al. (2015), if taken alone, suggests more AGN at a given bolometric luminosity. We further extrapolate the Lacy et al. (2015) fit to higher redshifts and lower luminosities than covered by their data.

Although we do not use them to constrain our model, we show JWST results at $z = 4, 5$ taken from Matthee et al. (2024) (as converted to bolometric luminosity by Habouzit (2024)) in Fig. 1. Data from Matthee et al. (2024) was broad-line selected from the FRESCO (Oesch et al. 2023) and EIGER surveys, and span $z = 4.2 - 5.5$. FRESCO and EIGER are spectroscopic slitless surveys with uniform selection in their fields, providing a complete sample with clear volume estimates. These results also hint towards a higher LF at high redshift than expected from the fit of Shen et al. (2020), in particular when taking into account that JWST is likely detecting only a subpopulation of all AGNs, and the obscured fraction could be as high as 80% (Gilli et al. 2022). We differentiate the lowest luminosity data point by plotting it in gray, as it is likely affected by incompleteness, see discussion in Matthee et al. (2024).

Other JWST observations (Harikane et al. 2023; Maiolino et al. 2023; Scholtz et al. 2023; Taylor et al. 2024) suggest an even larger population of faint AGN, although sample selections are not as clean as in slitless surveys. In Fig. 1, we show a lower bound to the LF at $z = 7$ obtained by Greene et al. (2024) using continuum-based selections. These results point in the direction of an even higher LF, but it should be noted that this type of selection may include also non-AGN sources (Pérez-González et al. 2024; Akins et al. 2024).

For the stochastic GW background, we use the results of the second data release from EPTA (Antoniadis et al. 2023a,b,c, 2024, 2023d), which are consistent with those of other PTAs (Agazie et al. 2024), see Fig. 2.

In this work, we do not fit for the $M_* - M_{\text{BH}}$ relation, but we perform a cross validation by comparing our results at $z = 0$ with

the fit from Greene et al. (2020) (‘All’, including scatter), which is based on a large compilation of galaxies. At higher redshifts, we compare to the fits from Pacucci et al. (2023), derived from JWST data at redshifts $z = 4$ to 7.

4.2. Computation of the likelihood and sampling

Given the current uncertainty on the LF, we wish to explore a scenario where the true LF lies somewhere between the fits proposed in Shen et al. (2020) and Lacy et al. (2015). We denote $\Phi_{\text{Lacy}}(L_{\text{BH}}, z_0)$ and $\Phi_{\text{Shen}}(L_{\text{BH}}, z_0)$ the mean of the fits from Lacy et al. (2015) and Shen et al. (2020) respectively, and $\sigma_{\text{Lacy}}(L_{\text{BH}}, z_0)$ and $\sigma_{\text{Shen}}(L_{\text{BH}}, z_0)$ their standard deviations (in log space). For a given redshift, we define a probability distribution $p_{\text{LF}}(\log_{10} \Phi, L_{\text{BH}}, z_0)$ that, in each luminosity bin, is flat between $\min(\log_{10} \Phi_{\text{Lacy}} - \sigma_{\text{Lacy}}, \log_{10} \Phi_{\text{Shen}} - \sigma_{\text{Shen}})$ and $\max(\log_{10} \Phi_{\text{Lacy}} + \sigma_{\text{Lacy}}, \log_{10} \Phi_{\text{Shen}} + \sigma_{\text{Shen}})$ and beyond these limits falls as a Gaussian with standard deviation σ_{Lacy} or σ_{Shen} accordingly.

Our likelihood for the LF of a given set of parameters Λ , $\mathcal{L}_{\text{LF}}(\Lambda, L_{\text{BH}}, z_0)$, is obtained by including the Poisson error on the LF computed from simulations so that

$$\mathcal{L}_{\text{LF}}(\Lambda, L_{\text{BH}}, z_0) = \int p(\Phi|\Lambda) p_{\text{LF}}(\log_{10} \Phi, L_{\text{BH}}, z_0) d\Phi, \quad (27)$$

where $p(\Phi|\Lambda)$ is a normal distribution with mean given by Eq. (11) and standard deviation Eq. (12). In practice, we perform a Monte-Carlo integration, drawing samples for Φ from this normal distribution, truncating to positive values of Φ .⁴ The total log-likelihood at z_0 is obtained by summing over the luminosity bins in a z_0 -dependent range:

$$\ln \mathcal{L}_{\text{LF}}(\Lambda, z_0) = \sum_{L_{\text{BH},\text{min}} \leq L_{\text{BH}} \leq L_{\text{BH},\text{max}}} \ln \mathcal{L}_{\text{LF}}(\Lambda, L_{\text{BH}}, z_0) \Delta L_{\text{BH}}. \quad (28)$$

Finally, the LF log-likelihood is obtained by summing over the different redshifts we wish to fit:

$$\ln \mathcal{L}_{\text{LF}}(\Lambda) = \sum_{z_0} \ln \mathcal{L}_{\text{LF}}(\Lambda, z_0). \quad (29)$$

Similarly, we use the EPTA posteriors (Antoniadis et al. 2023a,b,c, 2024, 2023d) on $\log_{10} \rho_c$, denoted by $p_{\text{PTA}}(\log_{10} \rho_c)$, to define the PTA likelihood in a given frequency bin f_0 as

$$\mathcal{L}_{\text{PTA}}(\Lambda, f_0) = \int p(\log_{10}(h_c)|\Lambda) p_{\text{PTA}}(\log_{10} \rho_c) d \log_{10} \rho_c. \quad (30)$$

We take $p(\log_{10}(h_c)|\Lambda)$ to be a normal distribution, with mean and error computed from Eqs. (21), (19), (20).⁵ We perform a Monte-Carlo integration using the samples of $p_{\text{PTA}}(\log_{10} \rho_c)$ provided with the EPTA data release.

⁴ Notice that we take the distribution on Φ to be normal, not on $\log_{10} \Phi$, since it is Φ that is a weighted sum of Poisson processes. Converting the error on Φ into an error on $\log_{10} \Phi$ through the standard propagation of errors is justified only when the error is much smaller than the quantity, which is not necessarily the case in the high luminosity bins where we have few counts, and would lead to underestimating the impact of Poisson errors. Ideally, we should use the formalism of Bohm & Zech (2014) rather than assuming a normal distribution when the total count is small and Poisson errors are large.

⁵ In this case, we assume a normal distribution on $\log_{10} \rho_c$ because the errors on ρ_c^2 is small enough so that propagation of error into $\log_{10} \rho_c$ can be used.

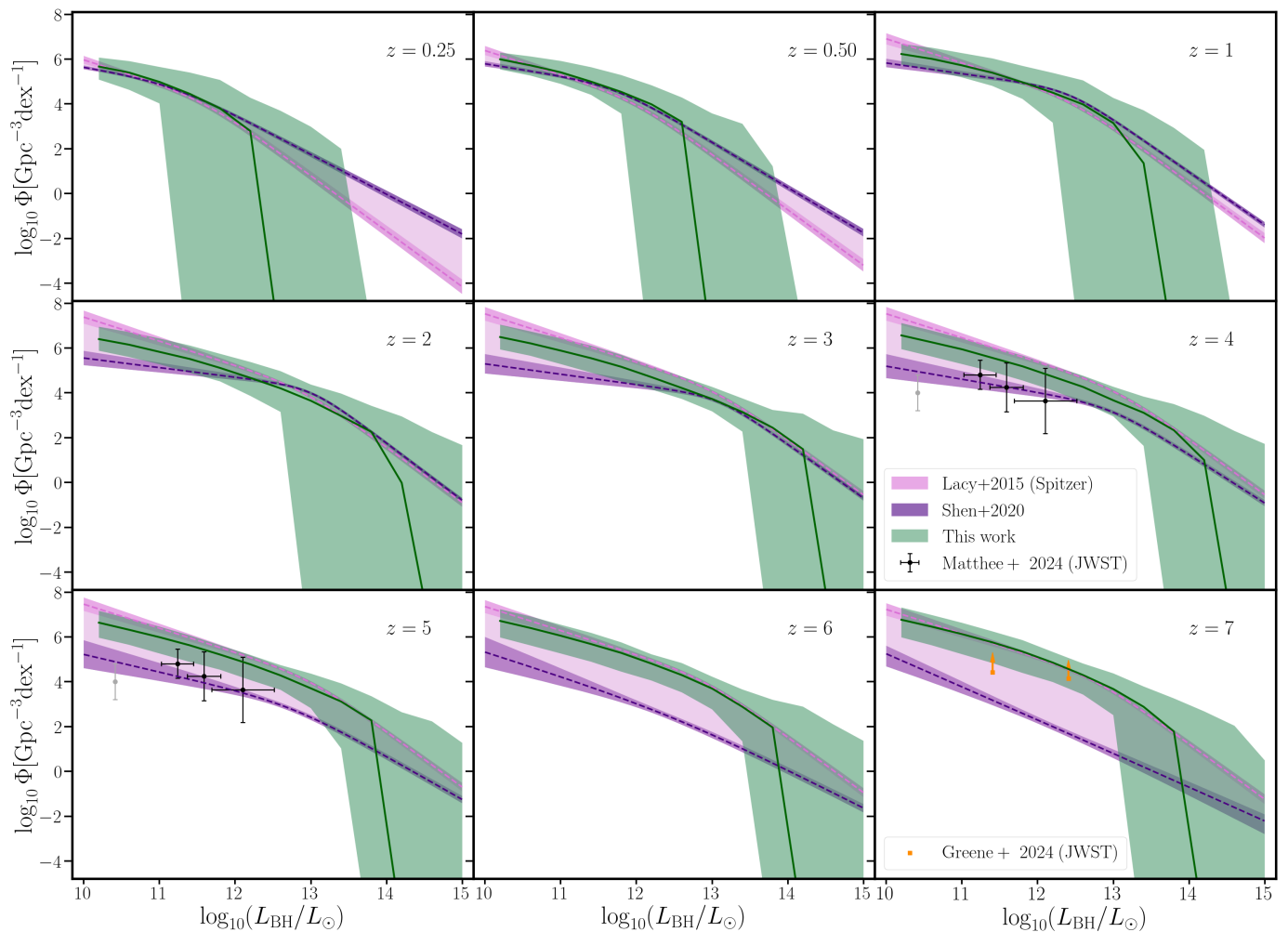


Fig. 1. The evolution of the luminosity function (LF). In green, we show the prediction of our model when fitting for the LF itself at redshifts 0.25, 0.5, 3 and 6, as well as for the GW background measured by EPTA, displaying the median (green line) and 90% confidence interval (green band). This should be compared with the fits to the observed LF from [Lacy et al. \(2015\)](#) (pink) and [Shen et al. \(2020\)](#) (purple) and the region in between (light pink), where we allow the observed LF to lie in our likelihood. At redshifts $z = 4, 5$ we also plot constraints from JWST (squares) from [Matthee et al. \(2024\)](#). The lowest luminosity point is shown in gray and not in black, because it is likely affected by incompleteness, see discussion in [Matthee et al. \(2024\)](#). At redshift $z = 7$, we plot a lower bound obtained by [Greene et al. \(2024\)](#) using JWST results. The recovered LF is remarkably consistent with observations, also at redshifts where we do not explicitly fit the data.

In this work, as a fiducial result, we fit the LF at $z = 0.25, 0.5, 3$ and 6 . For $z_0 = 0.25$, we fit in the range of luminosities $[10^{10}, 10^{11.5}]L_\odot$, for 0.5 , in the range $[10^{10}, 10^{12}]L_\odot$, while for $z_0 = 3$ and 6 , we fit in the range $[10^{12}, 10^{14}]L_\odot$ and $[10^{11.5}, 10^{13.5}]L_\odot$ respectively.

Since we assume MBH binaries to be on circular orbits, the slope of the GW background is constrained to $-2/3$, see Eq. (18). Therefore, fitting our model on the whole GW frequency range would give the EPTA data too large of a relative weight in the total fit, without giving it the flexibility to better accommodate the GW spectrum as a whole. To facilitate comparison with previous works ([Antoniadis et al. 2024](#); [Barausse et al. 2023](#)), and because the way we estimate the PTA spectrum – assuming a normal distribution – is more accurate at low frequencies ([Lamb & Taylor 2024](#)), we focus on the frequency bin at $f_0 = 1/(10 \text{ yr})$.

Finally, we assign zero likelihood to simulations that produce BHs at $z = 0$ with masses exceeding $10^{12}M_\odot$, as these are unrealistically massive. In our model, such BHs can form from heavy seeds, $\sim 10^6M_\odot$, which later accrete in burst mode with Eddington ratios reaching up to 10. By $z \sim 7$, these BHs typically have masses around $10^8\text{--}10^9M_\odot$, and since we limit accretion

only at lower redshifts, there is no mechanism to prevent them from continuing to grow, potentially reaching masses incompatible with observations. A more physically motivated accretion model – based on the available mass reservoir, rather than on Eddington ratios and accretion times – would likely prevent the formation of these excessively large BHs. However, since these are extreme outliers in our simulations (i.e., they appear in very few of the simulations that survive fitting to the LF and/or GW spectrum and in small numbers), we adopt this simple approach for now, leaving the implementation of a more refined accretion description for future work.

The priors used on the parameters of POMPOCO are detailed in Table 1. We explore the parameter space with an MCMC using the Eryn sampler ([Karnesis et al. 2023](#)). Since it is computationally cheap to run serially several sets of parameters for a given merger tree, we use many walkers (~ 500) and run the sampler only for a few steps (a few hundreds).

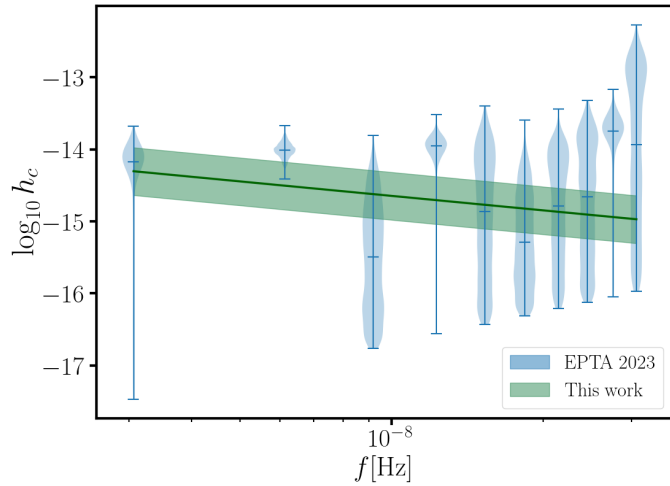


Fig. 2. The stochastic GW background predicted by our model, in green, and the free spectrum measured by EPTA, in blue. The 90% confidence intervals centred at the median for the amplitude of the GW background in the first and last bins i.e., at the frequencies 1/(10 yr) and 1/(1 yr), are $4.8^{+5.1}_{-2.7} \times 10^{-15}$ and $1.0^{+1.1}_{-0.6} \times 10^{-15}$, respectively. We recall that we fit only for the first frequency bin and that we assume MBH binaries to be circular, so that the slope of the GW background spectrum is fixed to $-2/3$. Our result is compatible with the EPTA data, although it suggests a slightly lower median value.

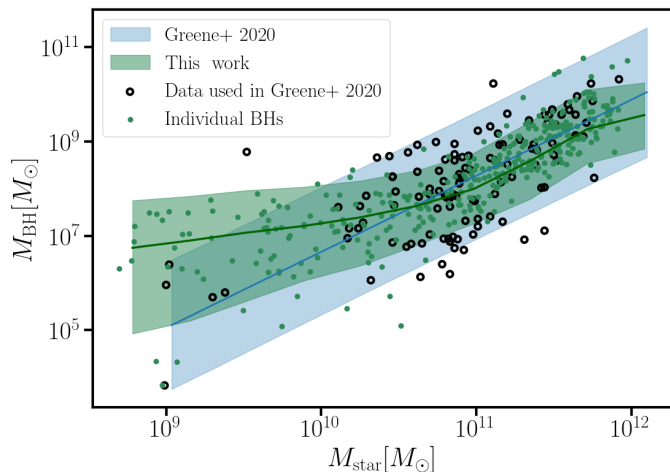


Fig. 3. Relation between the stellar mass and BH mass at redshift $z = 0$. We compare our results, in green, with the fit of the local relation from Greene et al. (2020) (‘all’), in blue, and the data also compiled in Greene et al. (2020), in black. Green points show a (random) subsample of BHs produced in our simulations, highlighting that our model can produce the most massive BHs in halos with $M_* \sim 10^{11} M_\odot$, while also producing MBHs of $10^7 - 10^{8.5} M_\odot$ in halos with $M_* \geq 10^{11} M_\odot$.

5. Combined fit to the luminosity function and the gravitational wave background

Our results for the LF, the GW background and the M_*-M_{BH} relation at $z = 0$ are shown in Fig. 1, 2 and 3 respectively. In each case, we present in green our model’s median (solid line) and 90% confidence interval (shaded region), as well as the observational data.

In Fig. 1, the light pink area denotes the region between the fits from Lacy et al. (2015) (pink) and Shen et al. (2020) (purple) where we allow the observational LF to reside. The recovered LF is remarkably consistent with observations at all redshifts –

including those for which we do not explicitly fit. Note that the break in our recovered LF at high luminosities is partially due to the finite number of dark matter halos we simulate.

The GW spectrum (Fig. 2) we recover aligns well with the EPTA data (in blue) though our median lies slightly lower. This suggests our results might be better compatible with the reduced amplitude of Goncharov et al. (2024), obtained by adopting an observationally-driven model for the pulsar noise. To facilitate comparison to Agazie et al. (2023a), we report the median of the GW background at two reference frequencies, together with the errors defining a 90% confidence region:

$$\begin{aligned} - h_c[1/(10 \text{ yr})] &= 4.8^{+5.1}_{-2.7} \times 10^{-15}, \\ - h_c[1/(1 \text{ yr})] &= 1.0^{+1.1}_{-0.6} \times 10^{-15}. \end{aligned}$$

As a comparison, if, instead of performing the fiducial fit to the LF and PTA described in Sec. 4.2, we use POMPOCO to fit only for the LF of Shen et al. (2020) across redshifts, we obtain the following estimates:

$$\begin{aligned} - h_c[1/(10 \text{ yr})] &= 3.9^{+7.0}_{-2.5} \times 10^{-16}, \\ - h_c[1/(1 \text{ yr})] &= 8.0^{+14.3}_{-5.1} \times 10^{-17}. \end{aligned}$$

The median values in the latter case are more than one order of magnitude below the ones reported above. Within the model itself, there is not so much the possibility of having a much lower LF at high z and producing a high GW background. In physical terms, a higher LF means higher density of BHs and so this is why the model can match the EPTA results. We recall that we assume MBH binaries to be circular, therefore the slope of the GW background spectrum is fixed to be $-2/3$, see Eq. (18). Including eccentricity and/or interactions with the environment would allow for a more flexible and shallower spectrum (Enoki & Nagashima 2007; Bonetti et al. 2018b; Antoniadis et al. 2024; Ellis et al. 2024a). We plan to explore these possibilities in future work.

The resulting M_*-M_{BH} relation at $z = 0$ (Fig. 3) is in good agreement with the fit from Greene et al. (2020) (in blue), particularly in the region where most of the observational data (black points) are concentrated. A random sub-sample of individual MBHs from our simulations (green dots) shows that our model is capable of producing the most massive BHs observed in galaxies with $M_* \sim 10^{11} M_\odot$, while also producing MBHs of $10^7 - 10^{8.5} M_\odot$ in galaxies with $M_* \geq 10^{11} M_\odot$. While these BHs are clear outliers, our model is able to reproduce them, a feature that some other models find challenging, as discussed in Habouzit et al. (2021). The median mass for BHs in galaxies with mass $M_* < 10^{10} M_\odot$ is of the order of $10^7 M_\odot$ and lies above observations. This is because the observations on which we are fitting the model constrain mostly what happens in more massive galaxies, while the low-mass end is almost unconstrained. As a consequence, the error broadens in this region and the median value is determined rather by the implicit prior the parametrisation choice imposes on the M_*-M_{BH} relation. We stress, however, that most observations in low-mass galaxies are within our 90% confidence region, and even the one outside can actually be reproduced as an outlier of the distribution. We could in principle also fit for the M_*-M_{BH} relation and improve these results, but we have checked that this potential overestimate of BHs with mass $10^7 M_\odot$ does not impact at all our results on the PTA background, which is fully dominated by BHs with mass $> 10^8 M_\odot$. Finally, we show the M_*-M_{BH} relation at higher redshift in Fig. A.1, in App. A.

Overall, our analysis demonstrates that observations of the LF and of the (likely) GW background observed by PTAs can

find a consistent description in our physical model, provided we allow for a more abundant population of AGN compared to global fits of the AGN LF based mainly on optical/UV/X-ray, pre-JWST data.

We show the posterior distribution of the parameters of our model in Fig. 4 and 5. For the sake of readability, the first figure shows the parameters controlling the seeding and merger delays, and the second figure those controlling accretion. We do not observe strong correlations between these two groups of parameters.

We obtain a relatively good constraint on the properties of halos that are seeded, coming from the abundance of BHs in the Universe at different redshifts (i.e., the normalisation of the LF). Our model suggests that $\sim 10\%$ of halos with $M_h \gtrsim 10^7 M_\odot$ at $z \sim 20$ should host an MBH seed.⁶ The range of values favoured for $M_{h,seed}$ is more compatible with the prediction of relatively heavy seed models for the formation of seeds (see Regan & Volonteri 2024, for an overview and discussion). We obtain a broad posterior on the mean seed mass μ_{seed} , but with a clear preference for $\mu_{seed} \gtrsim 10^3 M_\odot$, in better agreement with the predictions of non-extreme heavy seed models (Volonteri et al. 2021). The tendency towards large values of σ_{seed} suggests that we tend to prefer broad initial distributions for the mass seed. This is likely due to the need to accommodate observations spanning a broad range of MBH masses, together with the restrictive shape of the seed mass distribution currently adopted in POMPOCO (a single Gaussian). Allowing for a combination of seeding channels (e.g. each having its own μ_{seed} and σ_{seed}) might improve upon this, albeit at the cost of increasing the parameter space. We expect that LISA will allow us to better identify the contribution of different seeding channels compared to current observations (Gair et al. 2011; Sesana et al. 2011; Klein et al. 2016; Toubiana et al. 2021).

We find large delays in MBH mergers to be strongly disfavoured, with $t_{delay} \lesssim 1\text{Gyr}$ at 90% confidence. We recall this is an additional delay to the DF timescale following halo mergers and that we have considered a single value for all MBHs, without a mass or redshift dependence. Our findings are in line with those of Antoniadis et al. (2024); Barausse et al. (2023); Agazie et al. (2023a), which found that PTA observations favour MBH binaries merging efficiently following galaxy mergers.

Moving on to the accretion parameters, the posterior on γ_{burst} suggests a log-flat distribution for f_{Edd} in burst mode following major halo mergers, favouring the occurrence of super-Eddington accretion episodes. These burst episodes are estimated to last a few tens of Myr, in agreement with the findings from Hopkins et al. (2006); Capelo et al. (2015). The parameters of steady-mode accretion, in turn, are poorly constrained individually. However, the anti-correlation between μ_{steady} and σ_{steady} is so that $\sim 10\%$ of BHs accreting in this mode have $f_{Edd} > 10^{-2}$ and $\sim 4\%$ have $f_{Edd} > 10^{-1}$. If we label these as AGN, this suggests that the AGN fraction is in the range 4–10% at ‘cosmic noon’, which in our model corresponds to $z \sim z_{cut}$. This is in good agreement with observations in different parts of

⁶ These values should be interpreted with caution, in particular for f_{seed} , due to the finite resolution of our DM halo merger trees. The minimum mass we resolve at $z = 20$ is $\sim 2 \times 10^6 (M_{h,0}/10^{14}) M_\odot$. Thus, for the most massive halos with mass $10^{15} M_\odot$ at $z = 0$, the minimum resolved mass is above our best estimate for $M_{h,seed}$. However, since we allow all leaves above $z = 10$ to be seeded, halos that fall below the mass resolution before $z = 20$ could still be seeded. Moreover, such heavy halos are strongly suppressed by the Press-Schechter mass function and contribute little to our Universe. Therefore, we expect our estimates to be qualitatively meaningful, in particular for $M_{h,seed}$.

the electromagnetic spectrum, which suggest an AGN fraction at $z \sim 1-3$ in the range 1–10% (Aird et al. 2012; Trump et al. 2013; Donley et al. 2012). The strong correlations between γ_{burst} and t_{burst} and between μ_{steady} and σ_{steady} point to the fact that a more physically-driven approach to describe accretion, e.g., based on a reservoir tracking the amount of mass available to accrete, might be possible, allowing to reduce the number of parameters in our model. We leave this exploration for future work.

Finally, our results do support the anti-hierarchical hypothesis for the growth of MBHs, as we observe a clear preference for accretion to shut off below $z_{cut} \sim 2.5$ with $m_{cut,0} \sim 6 \times 10^6 M_\odot$. Although not very well constrained, the evolution parameter for the cut-off mass with redshift, α_{cut} , does seem to favour strictly positive values, leading to the estimate that accretion is suppressed at $z_{cut} \sim 2.5$ for MBHs with mass $\gtrsim 10^8 M_\odot$. The inferred value of z_{cut} is in good agreement with observations and more complete numerical simulations, which estimate the peak of accretion to be in the range $z = 2-3$ (Merloni 2004; Hirschmann et al. 2012, 2014). Using our $M_* - M_{BH}$ relation, we see that the preferred value of $m_{cut,0}$ corresponds to a stellar mass of $\sim 8 \times 10^{10} M_\odot$, in good agreement with where the break in the $M_h - M_*$ relation of Moster et al. (2010) lies, for $M_h \sim 10^{12} M_\odot$. This break has been interpreted as being due to the combined effect of the feedback from supernovae (in smaller halos) and AGNs (in larger halos) (Croton et al. 2006; Shankar et al. 2006; Bower et al. 2006; Somerville et al. 2008).

The fact that the inferred values of the parameters entering POMPOCO are overall in good agreement with findings from observations and/or more complete numerical simulations reinforces our confidence that our model is able to capture the key features driving the formation and evolution of MBHs and that our conclusions on the compatibility of the LF and the GW background are robust.

6. LISA predictions

Next, we turn to the predictions for LISA based on our fits to the LF and the GW stochastic background. We compute the rate as a function of MBH binary parameters, as well as the total rate, following the procedure described in Sec. 3.4. We restrict to events with signal-to-noise ratio (SNR) above 8, which we assume to be the threshold for detection. The SNR of the sources is computed assuming the ‘Proposal’ noise curve (Amaro-Seoane et al. 2017) and using the IMRPhenomXHM model (García-Quirós et al. 2020) for the waveform. Since we do not track the evolution of spins in our simulations, for simplicity, we attribute a spin 0 to both BHs in a binary when computing SNRs. We do not expect our results for the expected number of detections to be much affected by this choice, since spins, at the level of the whole population, introduce a second order correction to the detectability of the sources. For each event, we draw the sky location, the phase at coalescence, the polarisation and the inclination angle isotropically.

Figure 6 shows the posterior distribution of the merger rate per year, while Figs. 7 and 8 present this rate as a function of the total binary mass, m_t , and redshift, z , respectively. The thick lines represent the mean values, with the shaded regions indicating the 90% confidence intervals, and the thin lines illustrating individual realisations of our model. Our predictions for LISA cover a wide range, with the expected number of merger events varying from a few to thousands per year. Our best estimate of a few hundred events annually is consistent with the ‘Q3-nod’ model from Klein et al. (2016) and the ‘HS-SN-nod’ model from Barausse et al. (2020). These models assume that MBHs form from

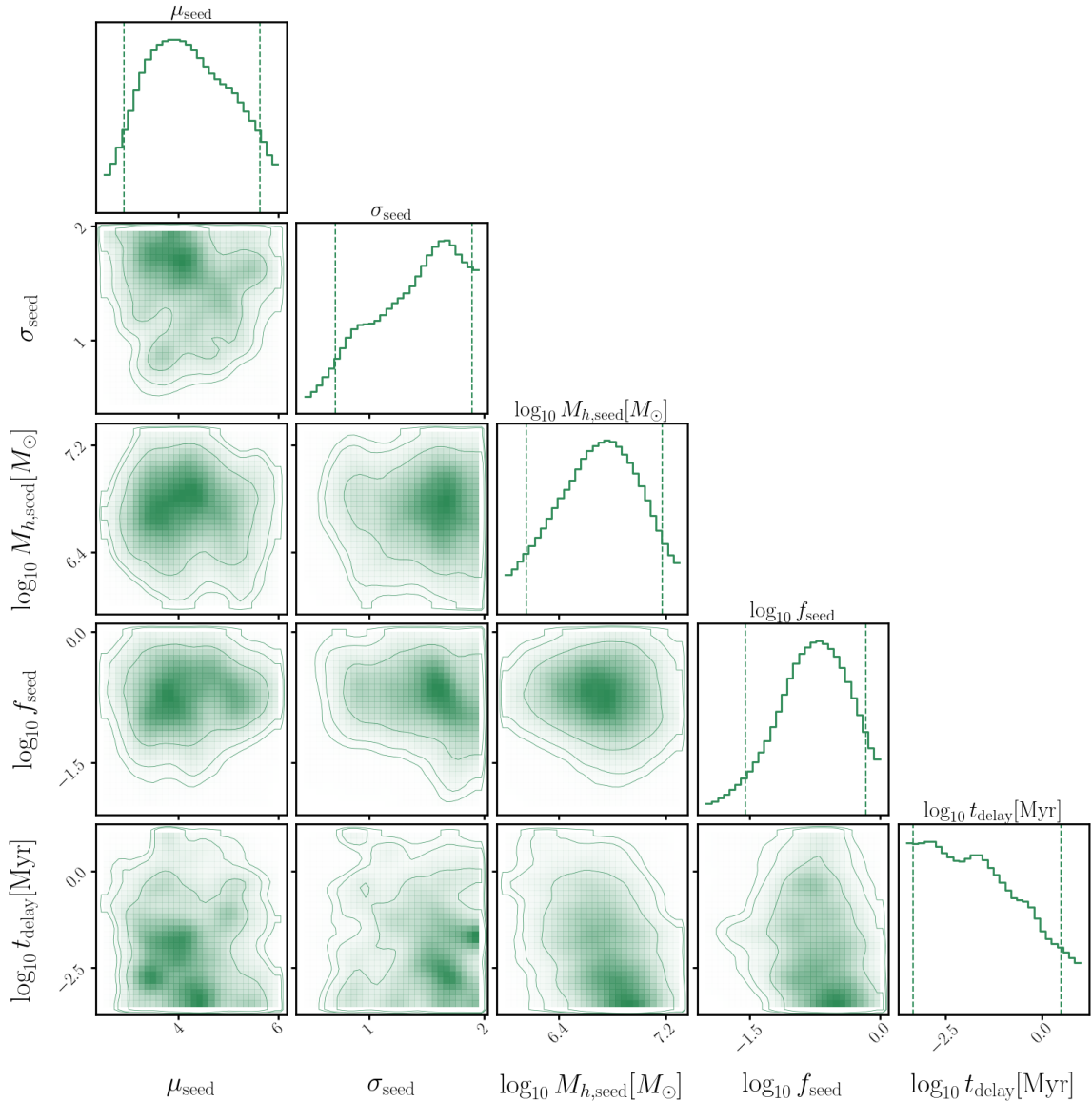


Fig. 4. Posterior on the model parameters related to seeding and BH mergers, when fitting for the LF and GW background. We show: the mean and standard deviation of the log-normal distribution of seed BH masses, μ_{seed} and σ_{seed} ; the minimum mass of halos seeded $M_{h,\text{seed}}$ and the seeding probability f_{seed} ; the delay of binary BH mergers (in addition to halo dynamical friction), t_{delay} .

heavy seeds (from the collapse of protogalactic disks (Volonteri et al. 2008)) and merge soon after galaxy mergers, which aligns well with the inferred values of μ_{seeds} and t_{delay} from our analysis. Those models also show agreement with the EPTA data (Antoniadis et al. 2024; Barausse et al. 2023).

The mass and redshift distributions in our predictions also align well with the Q3-nod and HS-SN-nod models, with peaks around $m_i \sim 3 \times 10^5 M_{\odot}$ and $z \sim 10$. The individual thin lines in Figs. 7 and 8 illustrate the diversity in the m_i distributions, with some peaking at lower masses and others at higher masses, and a similar pattern is seen in the redshift distributions. This demonstrates that, even in its current version, POMPOCO is flexible enough to describe a range of MBH populations – a key goal of the model. However, to fully exploit LISA’s potential to distinguish between different formation mechanisms, it will be necessary in the future to explicitly include more than one formation channel in our model.

7. Discussion and conclusions

In recent years, the number of observational probes into the population of MBHs in the Universe has been rapidly increasing, with even more expected in the near future. Preliminary results from JWST are already revealing intriguing discrepancies with previously accepted models, and it is anticipated that the upcoming observations will provide deeper insights. Additionally, PTA collaborations are on the verge of confirming the detection of the GW background in the nHz frequency band, generated by inspiralling MBH binaries. In the next decade, the launch of LISA will revolutionise our understanding of MBH formation and evolution by detecting a yet-unobserved population of merging MBHs. To fully capitalise on these upcoming observations, it is essential to develop a framework that can comprehensively compare theoretical predictions with a wide variety of observational data.

To this end, we have developed POMPOCO: Parametrisation Of the Massive black hole POPulation for Comparison to Observa-

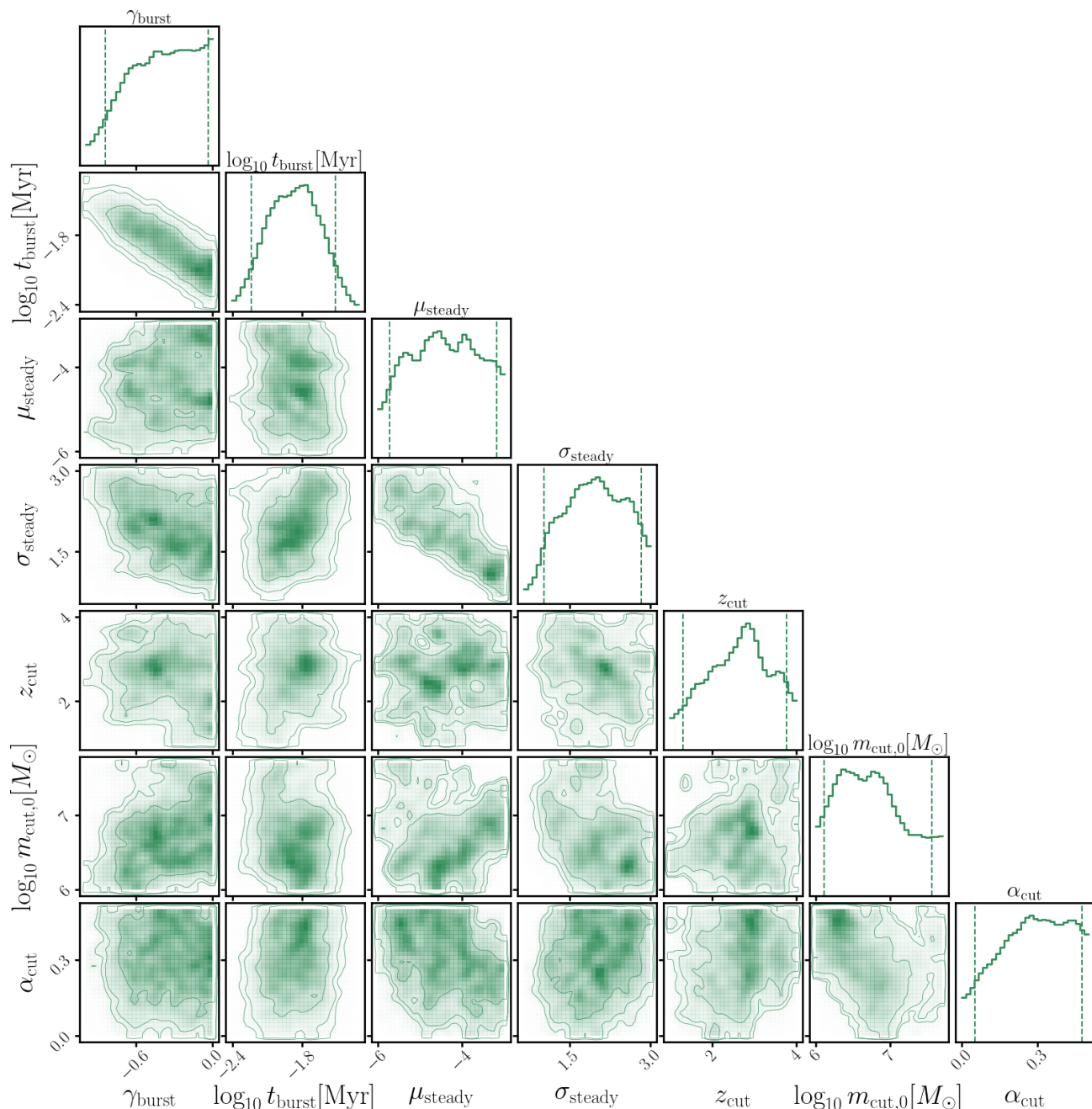


Fig. 5. Posterior on the model parameters related to accretion, when fitting for the LF and the GW background. We show: the slope of the power-law distribution γ_{burst} and the duration t_{burst} of burst accretion; the mean and standard deviation of the log-normal distribution of steady accretion rates, μ_{steady} and σ_{steady} ; the redshift z_{cut} below which accretion is shut off for heavier MBHs; the slope of the increase of the shut-off mass, $m_{\text{cut},0}$ at $z = 0$, with redshift, α_{cut} .

tions, a model that features 12 free parameters designed to effectively describe the formation and evolution of MBHs within DM halo merger trees. The computational efficiency of POMPOCO, compared to full cosmological simulations and SAMs, allows us to explore a wide range of parameter space and identify those configurations that best fit selected datasets.

In this study, we have used POMPOCO to demonstrate the consistency between the LF and the amplitude of the PTA GW background, particularly when allowing for an enhanced LF at high redshift, as suggested by extrapolating the results from Lacy et al. (2015) and by the preliminary findings from JWST (Harikane et al. 2023; Maiolino et al. 2023; Greene et al. 2024; Matthee et al. 2024; Taylor et al. 2024). (See also Somalwar &

Ravi (2023); Ellis et al. (2024b) for a similar analysis, also finding consistency between PTA observations and JWST black hole candidates.) To achieve this, we defined a likelihood function that accommodates the LF at different redshifts to lie between the comprehensive fits from Shen et al. (2020) and the fits to mid-IR observations from Lacy et al. (2015), and alongside the amplitude of the GW background inferred for the first frequency bin of the EPTA data. We then conducted a full Bayesian analysis. While our inferred GW spectrum is in clear agreement with the EPTA data, the median of our prediction lies slightly below theirs, potentially indicating a lower background, as proposed by Goncharov et al. (2024). Although we have focused on the case

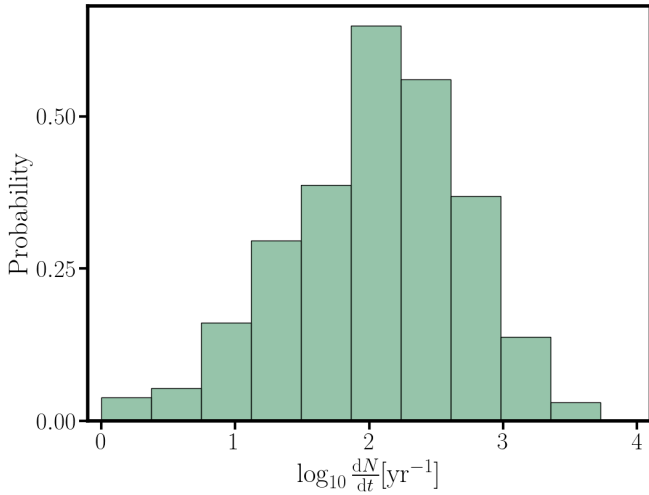


Fig. 6. Prediction of the rate of MBH mergers detectable by LISA per year, after fitting for the LF and the GW background measured by EPTA, assuming an SNR threshold of 8.

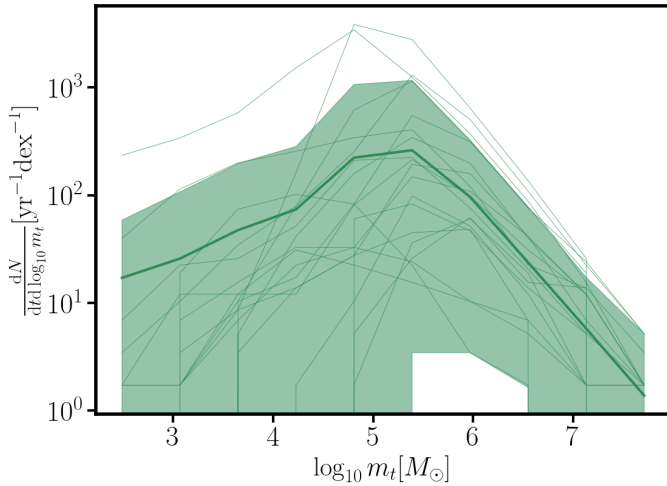


Fig. 7. Prediction of the rate of mergers detectable by LISA as a function of the total source-frame mass of the binary, assuming an SNR threshold of 8. Thick lines show the mean, the shaded area the 90% confidence region and thin lines individual realisations of our model after fitting for the LF and the GW background of EPTA.

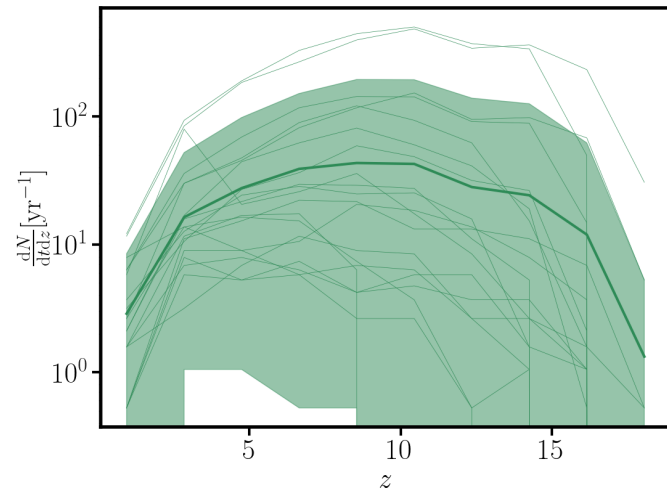


Fig. 8. Prediction of the rate of mergers detectable by LISA as a function of the redshift, assuming an SNR threshold of 8. See also Fig. 7.

of circular binaries in this work, we hope to include the effect of eccentricity when fitting to PTA data in future studies.

We verified our results against the observed $M_* - M_{\text{BH}}$ relation at $z = 0$, for which we do not explicitly fit, and observe an excellent agreement with the fit by [Greene et al. \(2020\)](#). Furthermore, our model is capable of reproducing even some of the MBHs observed outside of the main distribution, a feature that many models struggle with ([Habouzit et al. 2021](#)).

A key strength of POMPOCO lies in its ability to provide a posterior distribution for the model parameters when simultaneously fitting to the LF and the GW background. For instance, our Bayesian analysis showed that approximately $\sim 10\%$ of halos with mass $\geq 10^7 M_\odot$ at $z \sim 20$ should host an MBH seed, with characteristic masses ranging from 10^3 and $5 \times 10^6 M_\odot$. Additionally, we estimated that a fraction of MBHs undergoes super-Eddington accretion in burst episodes lasting a few tens of million years. At “cosmic noon”, we predict an AGN fraction of 4 – 10%, with the peak of accretion occurring at $z \sim 2.5$. Finally, we found that MBHs with masses $\geq 10^8 M_\odot$ should experience accretion suppression by $z \sim 2.5$, and that this suppression should extend to MBHs with masses $\geq 6 \times 10^6 M_\odot$ by $z = 0$. These estimates are consistent with the findings of more detailed numerical simulations and observations, suggesting that POMPOCO captures the essential features driving MBH formation and evolution.

Our model’s predictions for LISA are broad, yet consistent with existing SAMs, such as the Q3-nod model ([Klein et al. 2016](#)) and the SN-nodelays model ([Barausse et al. 2020](#)). These models assume that MBHs form from heavy seeds and merge efficiently following galaxy mergers. Furthermore, we find that POMPOCO exhibits the flexibility to describe a variety of populations of merging MBHs while remaining compatible with current observations. However, to fully leverage LISA’s potential to distinguish between different formation scenarios, we plan to increase the flexibility of the seed distribution in our model.

Looking ahead, we aim to introduce several improvements to POMPOCO. In addition to incorporating eccentricity and other formation channels, we plan to model the spin evolution of MBHs, which is critically sensitive to the environment of merging MBH binaries ([Berti & Volonteri 2008](#); [Sesana et al. 2014](#); [Spadaro et al. 2024](#)). Including eccentricity and spins will also allow us to correctly model the impact of kicks following MBH mergers, which we neglected in this work, and which could lower the LISA rates. Moreover, we intend to adopt a more physically motivated accretion model, such as one based on the mass reservoir available for accretion, which could reduce the parameter space and prevent the formation of unrealistically large MBHs. Addressing these issues will be crucial for fully extracting the astrophysical information encoded in LISA’s observations and realising the observatory’s immense potential ([Gair et al. 2011](#); [Klein et al. 2016](#); [Bonetti et al. 2019](#); [Toubiana et al. 2021](#); [Fang & Yang 2023](#); [Langen et al. 2024](#); [Spadaro et al. 2024](#)).

Acknowledgements

We are thankful to S. Grunewald for his precious help in making POMPOCO fit to run on the Hypatia cluster, to L. Speri for providing us the EPTA data, and to M. Habouzit for fruitful discussion. A.T. is supported by ERC Starting Grant No. 945155–GWmining, Cariplo Foundation Grant No. 2021-0555, MUR PRIN Grant No. 2022-Z9X4XS, MUR Grant “Progetto Dipartimenti di Eccellenza 2023-2027” (BiCoQ), and the ICSC National Research Centre funded by NextGenerationEU. E.B. acknowledges support from the European Union’s H2020 ERC

Consolidator Grant “GRavity from Astrophysical to Microscopic Scales” (Grant No. GRAMS-815673), the PRIN 2022 grant “GUVIRP - Gravity tests in the UltraViolet and InfraRed with Pulsar timing”, and the EU Horizon 2020 Research and Innovation Programme under the Marie Skłodowska-Curie Grant Agreement No. 101007855. L.S. acknowledges support from the UKRI guarantee funding (project no. EP/Y023706/1). MV acknowledges funding from the French National Research Agency (grant ANR-21-CE31-0026, project MBH_waves). This work has received funding from the Centre National d’Etudes Spatiales.

References

- Agazie, G. et al. 2023a, *Astrophys. J. Lett.*, 952, L37
- Agazie, G. et al. 2023b, *Astrophys. J. Lett.*, 951, L8
- Agazie, G. et al. 2024, *Astrophys. J.*, 966, 105
- Aird, J., Coil, A. L., Moustakas, J., et al. 2012, *ApJ*, 746, 90
- Akins, H. B., Casey, C. M., Lambrides, E., et al. 2024, arXiv e-prints, arXiv:2406.10341
- Allevato, V., Shankar, F., Marsden, C., et al. 2021, *The Astrophysical Journal*, 916, 34
- Amaro-Seoane, P., Audley, H., Babak, S., et al. 2017, *Laser Interferometer Space Antenna*
- Antoniadis, J. et al. 2023a, *Astron. Astrophys.*, 678, A48
- Antoniadis, J. et al. 2023b, *Astron. Astrophys.*, 678, A49
- Antoniadis, J. et al. 2023c, *Astron. Astrophys.*, 678, A50
- Antoniadis, J. et al. 2023d [arXiv:2306.16226]
- Antoniadis, J. et al. 2024, *Astron. Astrophys.*, 685, A94
- Baldassare, V. F., Geha, M., & Greene, J. 2020, *ApJ*, 896, 10
- Barausse, E. 2012, *Mon. Not. Roy. Astron. Soc.*, 423, 2533
- Barausse, E., Dey, K., Crisostomi, M., et al. 2023, *Phys. Rev. D*, 108, 103034
- Barausse, E., Dvorkin, I., Tremmel, M., Volonteri, M., & Bonetti, M. 2020, *Astrophys. J.*, 904, 16
- Benson, A. J. 2012, *New Astron.*, 17, 175
- Benson, A. J. 2017, *Mon. Not. Roy. Astron. Soc.*, 467, 3454
- Berti, E. & Volonteri, M. 2008, *Astrophys. J.*, 684, 822
- Bhowmick, A. K., Blecha, L., Torrey, P., et al. 2024, *MNRAS*, 531, 4311
- Binney, J. & Tremaine, S. 1987, *Galactic dynamics*
- Boettner, C., Trebitsch, M., & Dayal, P. 2023, arXiv e-prints, arXiv:2303.11368
- Bohm, G. & Zech, G. 2014, *Nucl. Instrum. Meth. A*, 748, 1
- Bond, J. R., Cole, S., Efstathiou, G., & Kaiser, N. 1991, *Astrophys. J.*, 379, 440
- Bonetti, M., Haardt, F., Sesana, A., & Barausse, E. 2018a, *Mon. Not. Roy. Astron. Soc.*, 477, 3910
- Bonetti, M., Sesana, A., Barausse, E., & Haardt, F. 2018b, *Mon. Not. Roy. Astron. Soc.*, 477, 2599
- Bonetti, M., Sesana, A., Haardt, F., Barausse, E., & Colpi, M. 2019, *Mon. Not. Roy. Astron. Soc.*, 486, 4044
- Bower, R. G. 1991, *Mon. Not. Roy. Astron. Soc.*, 248, 332
- Bower, R. G., Benson, A. J., Malbon, R., et al. 2006, *MNRAS*, 370, 645
- Capelo, P. R., Volonteri, M., Dotti, M., et al. 2015, *MNRAS*, 447, 2123
- Cole, S., Lacey, C. G., Baugh, C. M., & Frenk, C. S. 2002, *Monthly Notices of the Royal Astronomical Society*, 319, 168–204
- Colpi, M. 2014, *Space Sci. Rev.*, 183, 189
- Colpi, M. et al. 2024 [arXiv:2402.07571]
- Conroy, C. & White, M. 2012, *The Astrophysical Journal*, 762, 70
- Croton, D. J., Springel, V., White, S. D. M., et al. 2006, *MNRAS*, 365, 11
- Dayal, P., Rossi, E. M., Shiralilou, B., et al. 2019, *Monthly Notices of the Royal Astronomical Society*, 486, 2336–2350
- Donley, J. L., Koekemoer, A. M., Brusa, M., et al. 2012, *ApJ*, 748, 142
- Dubois, Y., Volonteri, M., & Silk, J. 2014, *Mon. Not. Roy. Astron. Soc.*, 440, 1590
- Ellis, J., Fairbairn, M., Hütsi, G., et al. 2024a, *Phys. Rev. D*, 109, L021302
- Ellis, J., Fairbairn, M., Hütsi, G., et al. 2024b [arXiv:2403.19650]
- Enoki, M. & Nagashima, M. 2007, *Prog. Theor. Phys.*, 117, 241
- Fabian, A. C. 2012, *ARA&A*, 50, 455
- Fang, Y. & Yang, H. 2023, *Mon. Not. Roy. Astron. Soc.*, 523, 5120
- Ferrarese, L. & Merritt, D. 2000, *ApJ*, 539, L9
- Gair, J. R., Sesana, A., Berti, E., & Volonteri, M. 2011, *Class. Quant. Grav.*, 28, 094018
- García-Quiros, C., Colleoni, M., Husa, S., et al. 2020, *Phys. Rev. D*, 102, 064002
- Gardner, J. P. et al. 2006, *Space Sci. Rev.*, 123, 485
- Gehren, T., Fried, J., Wehinger, P. A., & Wyckoff, S. 1984, *ApJ*, 278, 11
- Gilli, R., Norman, C., Calura, F., et al. 2022, *A&A*, 666, A17
- Goncharov, B., Sardana, S., Sesana, A., et al. 2024 [arXiv:2409.03627]
- Greene, J. E., Labbe, I., Goulding, A. D., et al. 2024, *ApJ*, 964, 39
- Greene, J. E., Strader, J., & Ho, L. C. 2020, *ARA&A*, 58, 257
- Habouzit, M. 2024, arXiv e-prints, arXiv:2405.05319
- Habouzit, M., Li, Y., Somerville, R. S., et al. 2021, *MNRAS*, 503, 1940
- Harikane, Y., Zhang, Y., Nakajima, K., et al. 2023, *ApJ*, 959, 39
- Hartwig, T. 2019, in *Formation of the First Black Holes (WORLD SCIENTIFIC)*, 161–175
- Hirschmann, M., Dolag, K., Saro, A., et al. 2014, *Mon. Not. Roy. Astron. Soc.*, 442, 2304
- Hirschmann, M., Somerville, R. S., Naab, T., & Burkert, A. 2012, *Mon. Not. Roy. Astron. Soc.*, 426, 237
- Hopkins, P. F., Hernquist, L., Cox, T. J., et al. 2006, *ApJS*, 163, 1
- Hopkins, P. F., Richards, G. T., & Hernquist, L. 2007, *Astrophys. J.*, 654, 731
- Izquierdo-Villalba, D., Bonoli, S., Dotti, M., et al. 2020 [arXiv:2001.10548]
- Izquierdo-Villalba, D., Sesana, A., Colpi, M., et al. 2024, *A&A*, 686, A183
- Kannan, R., Garaldi, E., Smith, A., et al. 2021, *Monthly Notices of the Royal Astronomical Society*, 511, 4005–4030
- Karnesis, N., Katz, M. L., Korsakova, N., Gair, J. R., & Stergioulas, N. 2023 [arXiv:2303.02164]
- Klein, A. et al. 2016, *Phys. Rev. D*, 93, 024003
- Kocevski, D. D., Barro, G., McGrath, E. J., et al. 2023, *ApJ*, 946, L14
- Kokorev, V., Fujimoto, S., Labbe, I., et al. 2023, *ApJ*, 957, L7
- Kormendy, J. & Ho, L. C. 2013, *Annual Review of Astronomy and Astrophysics*, 51, 511–653
- Kormendy, J. & Richstone, D. 1995, *Ann. Rev. Astron. Astrophys.*, 33, 581
- Kulier, A., Ostriker, J. P., Natarajan, P., Lackner, C. N., & Cen, R. 2015, *Astrophys. J.*, 799, 178
- Lacey, C. G. & Cole, S. 1993, *Mon. Not. Roy. Astron. Soc.*, 262, 627
- Lacey, M., Ridgway, S. E., Sajina, A., et al. 2015, *Astrophys. J.*, 802, 102
- Lamb, W. G. & Taylor, S. R. 2024, *Astrophys. J. Lett.*, 971, L10
- Langen, V., Tamanini, N., Marsat, S., & Bortolas, E. 2024 [arXiv:2409.06527]
- Latif, M. A. & Ferrara, A. 2016, *Publ. Astron. Soc. Austral.*, 33, e051
- Li, J., Silverman, J. D., Shen, Y., et al. 2024, arXiv e-prints, arXiv:2403.00074
- Lupi, A., Haardt, F., Dotti, M., et al. 2016, *MNRAS*, 456, 2993
- Lupi, A., Quadri, G., Volonteri, M., Colpi, M., & Regan, J. A. 2024, *A&A*, 686, A256
- Lyu, J., Alberts, S., Rieke, G. H., et al. 2024, *The Astrophysical Journal*, 966, 229
- Maiolino, R. et al. 2023 [arXiv:2308.01230]
- Mathee, J., Naidu, R. P., Brammer, G., et al. 2024, *ApJ*, 963, 129
- McConnell, N. J. & Ma, C.-P. 2013, *ApJ*, 764, 184
- Merloni, A. 2004, *MNRAS*, 353, 1035
- Monaco, P., Fontanot, F., & Taffoni, G. 2007, *MNRAS*, 375, 1189
- Moster, B. P., Somerville, R. S., Maulbetsch, C., et al. 2010, *ApJ*, 710, 903
- Ni, Y., Di Matteo, T., Bird, S., et al. 2022, *Monthly Notices of the Royal Astronomical Society*, 513, 670–692
- Oesch, P. A., Brammer, G., Naidu, R. P., et al. 2023, *MNRAS*, 525, 2864
- Onoue, M., Inayoshi, K., Ding, X., et al. 2023, *ApJ*, 942, L17
- Pacucci, F., Nguyen, B., Carniani, S., Maiolino, R., & Fan, X. 2023, *Astrophys. J. Lett.*, 957, L3
- Parkinson, H., Cole, S., & Helly, J. 2008, *Mon. Not. Roy. Astron. Soc.*, 383, 557
- Pérez-González, P. G., Barro, G., Rieke, G. H., et al. 2024, *ApJ*, 968, 4
- Phinney, E. S. 2001 [arXiv:astro-ph/0108028]
- Press, W. H. & Schechter, P. 1974, *Astrophys. J.*, 187, 425
- Reardon, D. J. et al. 2023, *Astrophys. J. Lett.*, 951, L6
- Rees, M. J. 1988, *Nature*, 333, 523
- Regan, J. & Volonteri, M. 2024, *The Open Journal of Astrophysics*, 7, 72
- Reines, A. E., Greene, J. E., & Geha, M. 2013, *Astrophys. J.*, 775, 116
- Reines, A. E., Sivakoff, G. R., Johnson, K. E., & Brogan, C. L. 2011, *Nature*, 470, 66
- Ricarte, A. & Natarajan, P. 2018, *Mon. Not. Roy. Astron. Soc.*, 474, 1995
- Ricarte, A., Tremmel, M., Natarajan, P., & Quinn, T. 2019, *MNRAS*, 489, 802
- Sahu, N., Graham, A. W., & Davis, B. L. 2019, *ApJ*, 876, 155
- Sassano, F., Capelo, P. R., Mayer, L., Schneider, R., & Valiante, R. 2023, *MNRAS*, 519, 1837
- Scholtz, J., Maiolino, R., D’Eugenio, F., et al. 2023, arXiv e-prints, arXiv:2311.18731
- Schramm, M. & Silverman, J. D. 2013, *The Astrophysical Journal*, 767, 13
- Scott, N., Graham, A. W., & Schombert, J. 2013, *The Astrophysical Journal*, 768, 76
- Sesana, A., Barausse, E., Dotti, M., & Rossi, E. M. 2014, *Astrophys. J.*, 794, 104
- Sesana, A., Gair, J., Berti, E., & Volonteri, M. 2011, *Phys. Rev. D*, 83, 044036
- Sesana, A., Vecchio, A., & Colacino, C. N. 2008, *Mon. Not. Roy. Astron. Soc.*, 390, 192
- Shankar, F. 2013, *Class. Quant. Grav.*, 30, 244001
- Shankar, F., Lapi, A., Salucci, P., De Zotti, G., & Danese, L. 2006, *Astrophys. J.*, 643, 14
- Shankar, F. et al. 2019 [arXiv:1910.10175]
- Shen, X., Hopkins, P. F., Faucher-Giguère, C.-A., et al. 2020, *Mon. Not. Roy. Astron. Soc.*, 495, 3252
- Shi, Y., Kremer, K., & Hopkins, P. F. 2024, arXiv e-prints, arXiv:2405.12164

- Small, T. A. & Blandford, R. D. 1992, *MNRAS*, 259, 725
- Smith, B. D., Regan, J. A., Downes, T. P., et al. 2018, *MNRAS*, 480, 3762
- Soltan, A. 1982, *MNRAS*, 200, 115
- Somalwar, J. J. & Ravi, V. 2023, arXiv e-prints, arXiv:2306.00898
- Somerville, R. S., Hopkins, P. F., Cox, T. J., Robertson, B. E., & Hernquist, L. 2008, *MNRAS*, 391, 481
- Somerville, R. S., Hopkins, P. F., Cox, T. J., Robertson, B. E., & Hernquist, L. 2008, *Monthly Notices of the Royal Astronomical Society*, 391, 481–506
- Spadaro, A., Buscicchio, R., Izquierdo-Villalba, D., et al. 2024 [arXiv:2409.13011]
- Springel, V., Pakmor, R., Pillepich, A., et al. 2017, *Monthly Notices of the Royal Astronomical Society*, 475, 676–698
- Tarafdar, P. et al. 2022, *Publ. Astron. Soc. Austral.*, 39, e053
- Taylor, A. J., Finkelstein, S. L., Kocevski, D. D., et al. 2024, arXiv e-prints, arXiv:2409.06772
- Toubiana, A., Wong, K. W. K., Babak, S., et al. 2021, *Phys. Rev. D*, 104, 083027
- Tremaine, S., Gebhardt, K., Bender, R., et al. 2002, *ApJ*, 574, 740
- Trinca, A., Schneider, R., Valiante, R., et al. 2022, *Monthly Notices of the Royal Astronomical Society*, 511, 616–640
- Trump, J. R., Hsu, A. D., Fang, J. J., et al. 2013, *ApJ*, 763, 133
- Tucci, M. & Volonteri, M. 2017, *Astron. Astrophys.*, 600, A64
- Volonteri, M., Dubois, Y., Pichon, C., & Devriendt, J. 2016, *Monthly Notices of the Royal Astronomical Society*, 460, 2979–2996
- Volonteri, M., Haardt, F., & Madau, P. 2003, *Astrophys. J.*, 582, 559
- Volonteri, M., Habouzit, M., & Colpi, M. 2021, *Nature Reviews Physics*, 3, 732
- Volonteri, M., Lodato, G., & Natarajan, P. 2008, *Mon. Not. Roy. Astron. Soc.*, 383, 1079
- Werner, M. W., Roellig, T. L., Low, F. J., et al. 2004, *ApJS*, 154, 1
- Xu, H. et al. 2023, *Res. Astron. Astrophys.*, 23, 075024
- Yu, Q. & Tremaine, S. 2002, *Monthly Notices of the Royal Astronomical Society*, 335, 965–976
- Zhang, H., Behroozi, P., Volonteri, M., et al. 2023, *MNRAS*, 518, 2123

Appendix A: $M_{\text{BH}} - M_*$ relation at higher redshifts

We compare in Fig. A.1 our results for the $M_* - M_{\text{BH}}$ relation at $z = 3$ and $z = 6$ to high- z fit from Pacucci et al. (2023), which is derived from JWST observations, and the $z = 0$ fit of Greene et al. (2020). We caution the reader that the underlying intrinsic $M_* - M_{\text{BH}}$ relation at high- z , once selection biases are accounted for, may be better consistent with local results than the fit of Pacucci et al. (2023), see Li et al. (2024), implying a large population of undetected MBHs and AGN with lower mass ratio between M_{BH} and M_* .

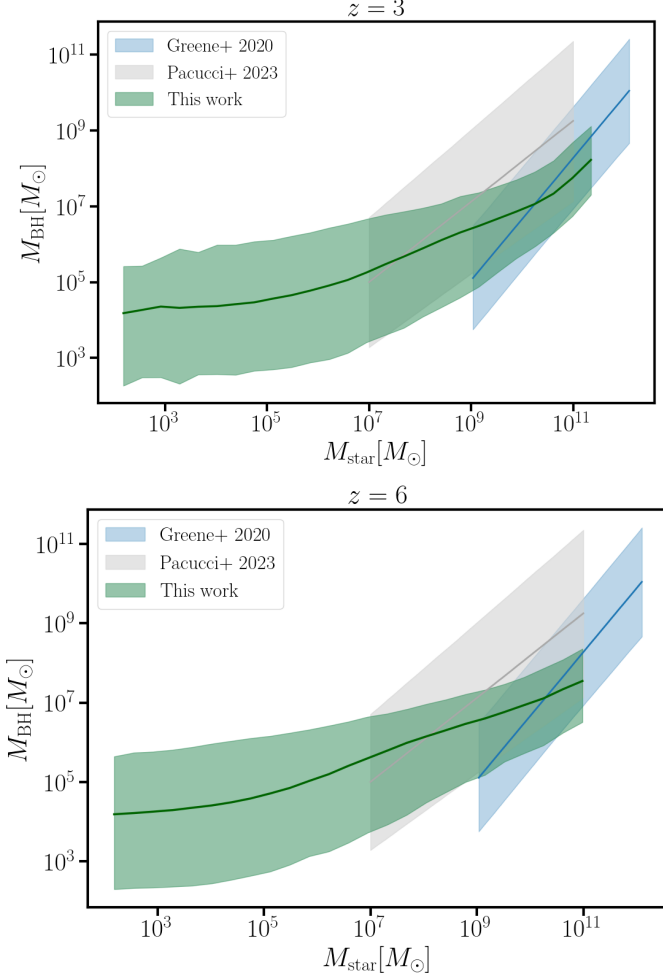


Fig. A.1. Relation between the BH mass and stellar mass at redshift $z = 3$ and 6. We compare our results (green) with the fit of the observed high- z relation (gray) of Pacucci et al. (2023) (based on JWST data at redshifts $z = 4$ to 7). For comparison, we also show the fit to the observed local relation (light blue) of Greene et al. (2020) ('all').